Cointegration strategy for damage assessment of offshore platforms subject to wind and wave forces

Kuai, H.; Civera, M.; Coletta, G.; Chiaia, B.; Surace, C.

DOI
10.1016/j.oceaneng.2024.117692

Publication date
2024

Document Version
Final published version

Published in
Ocean Engineering

Citation (APA)
Kuai, H., Civera, M., Coletta, G., Chiaia, B., & Surace, C. (2024). Cointegration strategy for damage assessment of offshore platforms subject to wind and wave forces. *Ocean Engineering*, *304*, Article 117692. https://doi.org/10.1016/j.oceaneng.2024.117692

Ocean Engineering 304 (2024) 117692

Contents lists available at ScienceDirect

Ocean Engineering

journal homepage: www.elsevier.com/locate/oceaneng

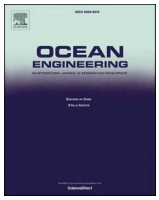

Research paper

Cointegration strategy for damage assessment of offshore platforms subject to wind and wave forces

H. Kuai [a,b], M. Civera [b,*], G. Coletta [b], B. Chiaia [b], C. Surace [b]

[a] Department of Geoscience & Engineering, Delft University of Technology, Stevinweg 1, Delft, Zuid-Holland, 2628 CN, the Netherlands
[b] Department of Structural, Building and Geotechnical Engineering, Politecnico di Torino, Corso Duca Degli Abruzzi 24, Torino, Italy

ARTICLE INFO

Keywords:
Offshore platform
Structural health monitoring (SHM)
Damage detection
Frequency domain decomposition (FDD)
Output-only monitoring
Relevance vector machine (RVM) regression

ABSTRACT

In structural engineering, offshore structures are undoubtedly among the most exposed to the effects of harsh environmental conditions. The external conditions of these semi-immersed systems involve complex combinations of wave and wind loads. The operating conditions are also unique because oil production platforms are subjected to repeated loading and unloading cycles of the extracted material, which continuously alter their mass. These characteristics make the definition of a structural health monitoring (SHM) protocol highly challenging but necessary to avoid environmental disasters. In this regard, this study discusses an SHM method that can be applied to offshore structures under realistic wave and wind loads. This approach combines anomaly detection, frequency domain decomposition, and a cointegration strategy. Two machine learning regression algorithms were tested to define a cointegration relationship: the support vector machine and the relevance vector machine. The effectiveness of the overall method was evaluated on time-domain signals generated from a finite-element model of a fixed steel platform, on which the Davenport and JONSWAP spectra were used to simulate wind and wave forces. The results show that this damage detection strategy is effective in supervising the health conditions in the analyzed scenario.

1. Introduction

Owing to their particular location, offshore platforms are exposed to extreme weather conditions such as downbursts and strong thunderstorms. These factors and others such as earthquakes, subsidence, and accidental collisions with ships, can cause structural damage, which can endanger the lives of operators and irreparably damage the ecosystems in which these platforms exist. For example, a downburst can cause a floating system to oscillate significantly, possibly causing damage (Nichol et al., 2021). Generally, structural damage arises from an accumulation of fatigue damage or sudden local collapse, which could impact the global static and dynamic behavior. For instance, in 1980, a storm hit the Norwegian North Sea, tearing five legs of the semi-submersible platform Alexander L. Kielland, resulting in the loss of 123 people. The accident investigation revealed that one bracing of the platform developed fatigue cracks before this extreme weather phenomenon, and the failure catastrophe began at this weak point (Almar-Naess et al., 1984).

Therefore, periodic inspections and/or continuous surveillance is required for all platform types. Consequently, structural health monitoring (SHM) and anomaly detection have received increasing attention for this type of structure (Ruotolo et al., 2000; Surace and Worden, 1998, 2010). SHM uses an automatic monitoring system, including sensors, data processors, and analysis terminals, to assess the health of platforms over time (Chen and Ni, 2018). This practice is quite different from nondestructive technologies (NDTs), such as X-ray, acoustic, or eddy currents, which can generally detect damage locally (Civera and Surace, 2022a). If global detection is required, using these techniques can take a long time and can be economically impractical. SHM techniques, particularly vibration-based inspection (VBI) (Rytter, 1993), are often used to obtain information on the global health status of structures. VBI detects changes in dynamic properties and analyzes the relationship between them and the occurrence of structural damage. This is generally performed using data processing techniques and damage-related features, ranging from the most basic (e.g., natural frequencies and mode shapes) to more refined parameters such as entropy (Civera and Surace, 2022b) or signal bicoherence (Civera et al., 2017), which quantify phase coupling within the signal (Hillis and Courtney, 2011).

For offshore platforms, recent methodologies reported in the

* Corresponding author.
E-mail address: marco.civera@polito.it (M. Civera).

https://doi.org/10.1016/j.oceaneng.2024.117692
Received 10 July 2023; Received in revised form 25 March 2024; Accepted 26 March 2024
Available online 16 April 2024

scientific literature include modal strain energy (Khosravan et al., 2021; Liu et al., 2017; Shen et al., 2015), frequency response functions (FRFs) (Fathi et al., 2020), and modal flexibility (Liu et al., 2018). However, these and other methods commonly used to assess platform damage are expensive and time-consuming (Pezeshki et al., 2023). For example, Liu et al. introduced an interesting damage detection method based on grouping modal strain energies and tested it on the results of a modal analysis carried out on a calibrated finite-element (FE) model of an offshore platform (Liu et al., 2017). Mojtahedi et al. validated an improved cross-model cross-mode (CMCM) iteration algorithm using experimental modal analysis (EMA) on a scaled-down laboratory model (Mojtahedi et al., 2020) naturally immersed in a controlled environment and conditions. Furthermore, the implementation of SHM for offshore structures faces significant challenges owing to the unpredictable and complex nature of wind and wave loads, and the frequent and significant changes in operating conditions driven by fluid extraction, which are generally not considered.

The importance of realistic operating conditions should not be understated. In fact, operating conditions may cause changes in dynamic characteristics similar to those caused by damage, generation of harmless and temporary false alarms, and much worse, masked real anomalies. Distinguishing the effects of damage from the effects of other factors, known as environmental and operational variations (EOVs) (Sohn, 2007), is a key aspect of VBI.

In this study, the management of EOVs and the related anomaly detection are addressed using the *cointegration* method associated with machine learning (ML) regression algorithms. This strategy has been tested in recent years in the SHM sector (Cross and Worden, 2011), particularly on civil, mechanical, and aerospace structures (Coletta et al., 2019; Dao et al., 2018; Liang et al., 2018; Sousa Tomé et al., 2020), but not yet in a case study involving an offshore platform and its unusual operating conditions. In particular, the support vector machine (SVM) and relevance vector machine (RVM) algorithms are selected to define the regression models required by the procedure. Dynamic data comprising the time series applied in cointegration were obtained using frequency domain decomposition (FDD), which is a simple and effective tool for system identification. A case study was conducted by simulating the behavior of a four-legged jacket platform under plausible ocean situations and operating conditions. Although it is a virtual model, this represents a compelling application because the symmetry and homogeneity of the material means that this offshore platform is more likely to have close natural frequencies than other more complex real structures, such as masonry buildings or reinforced concrete bridges.

1.1. Summary of the damage detection strategy with EOVs

One possible approach to monitoring the real health status of a structure while managing the presence of EOVs is to create a regression model that incorporates the behavior of dynamic characteristics that consider operating conditions such as mass and temperature changes. For example, consider a case in which the natural frequencies of a structure are selected as the diagnostic parameters. In a controlled environment, the dynamic characteristics remain unchanged (i.e., the time series of identified natural frequencies are stationary) if the normal structural conditions are maintained, whereas they change if damage, and therefore an alteration of stiffness, occurs.

Real structures are naturally exposed to uncontrolled external factors such as variable climatic or operational conditions. Thus, the natural frequencies fluctuate because of the EOVs, even if the structural conditions are normal. Their mechanisms of change can be captured using a regression model if a sufficiently large database is provided for training. If the database contains almost all operating conditions, the regression model rebuilds the change mechanism of the natural frequencies for all possible factors not related to damage. This model can then be used throughout the life of the structure to predict health behaviors as the observed input factors change. Once the observed trend of one (or more) of these fundamental natural frequencies deviates considerably from the predicted trend, the structure is no longer in its normal condition, which could result from the appearance of damage (according to the classic idea of damage detection as a matter of novelty detection) (Sohn et al., 2001).

This approach has not yet been applied to offshore platforms, probably because of the difficulties associated with their complex and specific environmental and operating conditions related to the variable mass of the extracted fluid, external temperature, and other relevant factors. For this type of construction, the variation in mass owing to the quantity of extracted material can be significant and can therefore lead to significant fluctuations in the modal parameters, given their close relationship. A positive aspect of SHM applications is that mass monitoring is generally performed routinely, making it easy and economical to obtain such data. Therefore, this study also involves mass data in the structural response model, which represents a difference, as well as an original aspect, compared to SHM procedures for civil structures, such as buildings and bridges, where the mass alteration under operating conditions could be less significant or less easily obtainable.

From a practical perspective, the proposed method relies solely on the use of the output-only recordings of a structure under normal operating conditions. In other words, it is not limited by any analytical model or strong assumption of the expected dynamic behavior; it can be directly applied on-site and does not require any interruption of the extraction process.

The remainder of this paper is organized as follows: Section 2 introduces the task of natural frequency identification from output-only readings, focusing on the FDD algorithm. It also extends its use to general inputs for offshore platforms. Section 3 presents the basic theory of cointegration and the SVM/RVM used to build the regression models. Section 4 describes the fixed platform FE model used in the case studies and the applied force model. Section 5 presents the entire procedure for clarifying the damage detection method. The results are presented in Section 6, followed by the discussion and conclusions in Sections 7 and 8, respectively.

2. Natural frequency identification

Two modal analysis strategies can be applied to obtain the vibrational properties of offshore platforms (or any other structures). The first is the most common: EMA, which requires that both the excitation forces and dynamic response of the platforms are known (Ewins, 2000). However, the continuous monitoring of excitation forces is costly and/or impractical. Therefore, operational modal analysis (OMA) is widely used in permanent monitoring systems. OMA relies solely on the output data to obtain the modal parameters of the entire structure (Peeters and Roeck, 2001).

2.1. Frequency domain decomposition (FDD)

Various OMA techniques have been developed to obtain vibrational properties. Peak picking is one of the simplest techniques, which accounts for its common use. This is conventionally applied under the assumption of white Gaussian noise (WGN) input (Varahram et al., 2019); however, it has been extended to and validated for platforms under realistic wind and wave forces (Ibrahim et al., 1996). According to some hypotheses (see Section 2.2), the FRF is proportional to the spectrum of the response signal acquired at that point. In summary, by representing the acquired acceleration time series in the frequency domain, the prevailing peaks in the spectrum can be used to estimate the natural frequencies of the underlying structure (Naderpour and Fakharian, 2016).

Peak picking is a well-established vibrational property estimation method for well-separated modes. However, if similar modes exist in a structure, they may be difficult to distinguish. Therefore, in this study, FDD, an extension of the peak-picking method, was employed, as out-

lined in (Varahram et al., 2019). The FDD method represents the power spectral density (PSD) of the response using a matrix where nonzero values occur only at discrete frequencies. Using singular value decomposition (SVD), the PSD matrix is decomposed as

$$\boldsymbol{G} = \boldsymbol{U}\Sigma\boldsymbol{V}^T \tag{1}$$

where $\boldsymbol{U}$ and $\mathbf{V}$ are two orthogonal matrices of the same dimension.

$\boldsymbol{\Sigma}$ is a diagonal matrix containing singular values of the PSD matrix.

The singular values are significant in relation to the modal participation factor and the positions of the peaks in the SVD correspond to the natural frequencies.

2.2. General random inputs

Importantly, the FDD was derived under the assumption of WGN excitation. However, for offshore platforms, the forces most frequently encountered, that is, wave and wind forces, cannot be considered WGN. A solution based on a load filter system was proposed in the literature (Brincker, 2014; Ibrahim et al., 1996). Random forces are assumed to be generated through a load filter. This load filter does not change the properties of the analyzed structures. Therefore, although the forces are generally random inputs, the entire procedure remains valid to deal with them. One aspect that needs to be considered is the separation between the vibrational content of the dynamic loads and the structure, which will be addressed and explained in subsequent sections when selecting the modes to be included in the cointegration analysis.

3. Cointegration

The concept of cointegration, initially introduced in econometrics (Engle and Granger, 1987), provides an indicator of a given phenomenon of interest (damage) that retains its sensitivity while being less susceptible to the influence of unwanted confounding factors (EOVs).

It identifies common trends within two or more series and can be used for SHM purposes by relating the common trends of the system's dynamic response and operating conditions that lead to changes in the dynamic characteristics. Therefore, as mentioned previously, the aim of using ML regression models is to estimate the relationship between the natural frequencies and operating conditions. This relationship can then be applied to cleanse the time series of the natural frequencies from EOVs not related to damage and thus helps assess the potential occurrence of damage (Shi et al., 2016).

In this framework, each series is characterized by the order of integration. It can be defined as the number of times a nonstationary time series needs to be differentiated to become stationary. Based on this theory, in 1987, Engle and Granger introduced a definition of linear cointegration: if two or more nonstationary time series have the same order of integration and there exists one stationary linear combination, then these time series are called cointegrated (Engle and Granger, 1987).

3.1. Augmented dickey-fuller test

The augmented Dickey–Fuller (ADF) test can be performed to determine the stationarity and order of integration of the time series. Considering time series x, the test involves fitting a model of the variable in the following form:

$$\Delta x_t = \alpha + \gamma t + \beta x_{t-1} + \sum_{i=1}^{m} \theta_i \Delta x_{t-i} + u_i; \Delta x_t = x_t - x_{t-1} \tag{2}$$

where α is the constant term.

γt is the deterministic trend term.

u_t is the residual term.

βx_{t-1} and $\sum_{i=1}^{m} \theta_i \Delta x_{t-i}$ are the lag terms.

The ADF test is based on the estimation of t statistic to test the null hypothesis of β

$$t = \widehat{\beta}/\sigma_\beta \tag{3}$$

where $\widehat{\beta}$ is the estimate of the β.

σ_β is the variance of $\widehat{\beta}$.

The results obtained using the formula above were compared with the critical values provided by Dickey and Fuller (2008). If the t statistic is smaller than the critical values, then the null hypothesis of β (i.e., it contains a unit root) can be rejected. This means that the corresponding time series is stationary; otherwise, the null hypothesis is accepted in favor of the alternative, implying that the tested time series is nonstationary (Perman, 1991; Shi et al., 2016).

3.2. Supervised learning models

As stated before, to apply cointegration, there are two main implementation steps: (1) ensuring that the involved time series have the same order of integration and (2) finding a proper stationary relationship. The ADF test solves the problem of determining the order of integration. At this point, estimating the stationary combination is a key point to address.

Several methods have been developed to achieve this. A good strategy is to create a regression model of one of the characteristics of the system using the others as predictors, and then use the residual of the model as a cointegration relationship. In fact, the residual could take on the meaning of a cointegration relation, because it is a combination of all the original nonstationary series, that is, the predicted characteristics and the predictors. There are many methodologies for implementing regression; here, as previously mentioned, SVM and RVM were applied. The theory of these two algorithms is well established in the scientific literature. However, to make this paper self-contained, the key passages are briefly recalled, starting with the SVM regression (Drucker et al., 1996; Shen et al., 2013).

3.2.1. SVM regression

The SVM is a well-known statistical method for classification and regression. Considering a training dataset of N inputs $\boldsymbol{x}_i$ and outputs y_i time series, the generalizing function, which considers the possible mapping of data into a higher-dimensional feature space, is defined as

$$f(\boldsymbol{x}_i) = \boldsymbol{w}^T \cdot \varphi(\boldsymbol{x}_i) + b \tag{4}$$

where $\mathbf{w}$ is the weights.

$\varphi(\boldsymbol{x}_i)$ is the mapping function, which can be linear or nonlinear, according to the addressed problem.

b is the constant term.

The objective of the SVM is to ensure that the result can cover as many observations (i.e., data points) as possible. If the distance between the decision boundary and the hyperplane is ε, this object can be described as

$$|f(\boldsymbol{x}_i) - y_i| \le \varepsilon \tag{5}$$

Based on the above formula, an ε-insensitive cost function is defined:

$$L_\varepsilon(f(\boldsymbol{x}_i) - y_i) = \begin{cases} |f(\boldsymbol{x}_i) - y_i| - \varepsilon, if\ |f(\boldsymbol{x}_i) - y_i| > \varepsilon \\ 0, if\ |f(\boldsymbol{x}_i) - y_i| \le \varepsilon. \end{cases} \tag{6}$$

Therefore, the optimization problem can be defined as

$$\min \quad \frac{1}{2}\|\boldsymbol{w}\|^2 + C\sum_{i=1}^{N} L_\varepsilon(f(\boldsymbol{x}_i) - y_i) \tag{7}$$

s.t. $y_i - \boldsymbol{w}^T \cdot \varphi(\boldsymbol{x}_i) - b \le \varepsilon$.

$\boldsymbol{w}^T \cdot \varphi(\boldsymbol{x}_i) + b - y_i \le \varepsilon$.Where C is a regularization constant.

Because some errors can be tolerated in the optimization problem, soft margins are proposed, and the optimization problem can be rewritten as

$$\min \quad \frac{1}{2}\|\boldsymbol{w}\|^2 + C\sum_{i=1}^{N}(\xi_i + \widehat{\xi}_i) \tag{8}$$

$s.t.\ y_i - \boldsymbol{w}^T\cdot\varphi(\boldsymbol{x}_i) - b \le \varepsilon + \xi_i.$

$\boldsymbol{w}^T\cdot\varphi(\boldsymbol{x}_i) + b - y_i \le \varepsilon + \widehat{\xi}_i.$

$\xi_i, \widehat{\xi}_i \ge 0$.Where $\xi_i, \widehat{\xi}_i$ are the so-called slack variables; as mentioned, these are introduced to allow for soft margins, i.e. to manage the errors.

By solving the optimization problem to determine $\boldsymbol{w}$ and b, one can obtain the decision function to predict the outputs. To create an accurate model, the algorithm requires C and ε tuning, which establish a balance between model flatness and overfitting: in this case, as per practice, these hyperparameters were defined through an optimization process based on the minimization of a 10-fold cross-validation loss.

3.2.2. RVM regression

To create appropriate regression models, the SVM uses an unconstrained number of support vectors. In some cases, their number can grow to an extent that leads to a high computational burden, especially when the training set is particularly large (Tipping, 2001). This may hamper reliable damage detection. Therefore, RVMs have been proposed to avoid these drawbacks. In this algorithm, a Bayesian approach is applied (Tipping, 2001).

Consider a prediction model of the regression that has the following function:

$$y_i = f(\boldsymbol{x}_i, \boldsymbol{w}) + \varepsilon_i = \boldsymbol{w}^{\boldsymbol{T}}\cdot\varphi(\boldsymbol{x}_i) + \varepsilon_i \tag{9}$$

where ε is a mean-zero Gaussian noise whose variance is β^{-1}.

The outputs of the model contain simultaneous signals and noise, and a Gaussian distribution of the likelihood of the prediction model is assumed:

$$p(y_i|\boldsymbol{x}_i, \boldsymbol{w}, \beta) = \mathcal{N}\left(y_i|\boldsymbol{w}^{\boldsymbol{T}}\cdot\boldsymbol{\varphi}(\boldsymbol{x}_i), \beta^{-1}\right) \tag{10}$$

For a set of data tests, $\mathbf{D}_m = (\mathbf{X}_m, \mathbf{Y}_m)$ containing inputs and outputs: $\mathbf{X}_m = (\mathrm{x}_1, \ldots, \mathrm{x}_m)$ and $\mathbf{Y}_m = (\mathrm{y}_1, \ldots, \mathrm{y}_m)$:

$$p(\boldsymbol{Y}_m|\boldsymbol{X}_m, \boldsymbol{w}, \beta) = \prod_{i=1}^{m}\mathcal{N}\left(y_i|\boldsymbol{w}^{\boldsymbol{T}}\cdot\boldsymbol{\varphi}(\boldsymbol{x}_i), \beta^{-1}\right) \tag{11}$$

Expressing Equation (11) in matrix form:

$$p(\boldsymbol{Y}_m|\boldsymbol{w}, \beta) = \mathcal{N}\left(\boldsymbol{Y}_m|\boldsymbol{w}^{\boldsymbol{T}}\cdot\Phi(\mathbf{x}), \beta^{-1}\boldsymbol{I}\right) \tag{12}$$

where $\boldsymbol{w} = (w_0, \ldots, w_m)$ is the weights matrix.

$\boldsymbol{\Phi}$ is the design matrix, the element of which is expressed by: $\varphi_{ij} = K(\boldsymbol{x}_i, \boldsymbol{x}_{j-1})$ and $\varphi_{i1} = 1$.

At the same time, the prior is assumed to follow the mean-zero Gaussian distribution and depends on the hyperparameters α:

$$p(\boldsymbol{w}|\boldsymbol{\alpha}) = \mathcal{N}(\boldsymbol{w}|\mathbf{0}, \boldsymbol{A}) \tag{13}$$

where $\boldsymbol{A} = diag(\alpha_0, \ldots, \alpha_m)$.

$\boldsymbol{\alpha} = (\alpha_0, \ldots, \alpha_m)$.

Because both the prior and likelihood follow a Gaussian distribution, the normalizing integral inside Bayes' rule is easy to obtain and is a convolution of Gaussians. Applying Bayes' rule, the posterior over-weight vectors obtained based on the above two equations can be represented by

$$p(\boldsymbol{w}|\boldsymbol{Y}_m, \boldsymbol{\alpha}, \beta) = \mathcal{N}(\boldsymbol{w}|\boldsymbol{\omega}_m, \boldsymbol{S}_m) \tag{14}$$

$$\boldsymbol{\omega}_m = \beta\boldsymbol{S}_m\Phi^T\boldsymbol{Y}_m \tag{15}$$

$$\boldsymbol{S}_m = \left(\boldsymbol{A} + \beta\Phi^T\boldsymbol{\Phi}\right)^{-1} \tag{16}$$

where $\boldsymbol{S}_m$ is the covariance of the posterior.

$\boldsymbol{\omega}_m$ is the mean of the posterior.

The above posterior is the distribution over the weights, given the observed data, hyperparameter, and noise variance. However, for this model, the hyperparameters and noise variance are unknown. Therefore, the posterior over all the unknowns is actually $p(\boldsymbol{w}, \boldsymbol{\alpha}, \beta|\boldsymbol{Y}_m)$, and can be expressed as

$$p(\boldsymbol{w}, \boldsymbol{\alpha}, \beta|\boldsymbol{Y}_m) = p(\boldsymbol{w}|\boldsymbol{Y}_m, \boldsymbol{\alpha}, \beta)p(\boldsymbol{\alpha}, \beta|\boldsymbol{Y}_m) \tag{17}$$

For Equation (17), the first term on the right-hand side is known and the second term needs to be defined. In practice, calculating the second term is impossible. The most frequently used method is to fix two unknowns to the most probable $\widehat{\boldsymbol{\alpha}}$ and $\widehat{\beta}$. Moreover, due to the definition $p(\boldsymbol{\alpha}, \beta|\boldsymbol{Y}_m) \propto p(\boldsymbol{Y}_m|\boldsymbol{\alpha}, \beta)p(\boldsymbol{\alpha}, \beta)$ and the fixed value for $\boldsymbol{\alpha}$ and β, the purpose of finding these two values can be transformed to maximize the term $p(\boldsymbol{Y}_m|\boldsymbol{\alpha}, \beta)$, which is known as evidence for the hyperparameters. Based on Equations (12) and (13), the following function can be obtained. Because the two terms on the right-hand side both follow the Gaussian distribution, the integral is a convolution of Gaussians, which can be easily calculated.

$$p(\boldsymbol{Y}_m|\boldsymbol{\alpha}, \beta) = \int p(\boldsymbol{Y}_m|\boldsymbol{w}, \beta)p(\boldsymbol{w}|\boldsymbol{\alpha})d\boldsymbol{w} = \mathcal{N}(\boldsymbol{Y}_m|\mathbf{0}, \boldsymbol{C}) \tag{18}$$

$$\boldsymbol{C} = \beta^{-1}\boldsymbol{I} + \Phi\boldsymbol{A}^{-1}\Phi^T \tag{19}$$

After differentiating this formula with respect to $\boldsymbol{\alpha}$ and β individually and applying them iteratively until the convergence criteria are satisfied, these two parameters can be obtained. The terms within the vector $\boldsymbol{\alpha}$ will notify the user to prune or preserve the corresponding basis functions. If α_i tends to infinity, then the corresponding $p(w_i|\boldsymbol{Y}_m, \boldsymbol{\alpha}, \beta)$ peak at zero, thus the corresponding vector should be pruned, saving computation cost (Tipping, 2001). The remaining vectors are referred to as relevance vectors.

Finally, the predictions are made based on the distribution over weights given the most probable value of $\widehat{\boldsymbol{\alpha}}$ and $\widehat{\beta}$. For a new test x*, the corresponding predicted output y* is expressed in terms of the predictive distribution

$$p(y^*|\boldsymbol{Y}_m, \widehat{\boldsymbol{\alpha}}, \widehat{\beta}) = \int p(y^*|\boldsymbol{w}, \widehat{\beta})p(\boldsymbol{w}|\boldsymbol{Y}_m, \widehat{\boldsymbol{\alpha}}, \widehat{\beta})d\boldsymbol{w}. \tag{20}$$

4. Case study

4.1. Platform FE model

To test the effectiveness of this damage detection method, several damage scenarios and operating conditions were considered as case studies based on a FE model of a steel jacket platform generated using the commercial software ANSYS 2020 R2. The concept and structural deisgn of this steel platform is similar to those adopted in previous studies (Surace and Worden, 1998). The geometric details are shown in Fig. 1. Sea level was set in the middle of the platform (indicated by 0 in Fig. 1) to obtain the results of the combined effects of waves and winds acting on the bottom and top halves of the structure. The red zone indicates the platform-splash zone. To simulate the damage, the structural elements inside this zone (except for the boundary elements) were altered according to several different scenarios, which are described later.

The supporting structure of the whole platform is composed of steel piles with an outside diameter of 0.7 m. A PIPE288 element, which considers Timoshenko beam theory for slender to moderately thick pipe structures, was chosen as its simulating element. At the top of the structure, the work plane of the platform was simulated using a SHELL181 element, considering the Mindlin plate theory. A linear model was considered in these case studies for the structure-soil-foundation interactions, assuming a Winkler foundation. Fig. 1 b shows the rear and front sides of the structure (defined according to the assumed direction of the incoming sea waves; this is discussed in later sections dedicated to the input force).

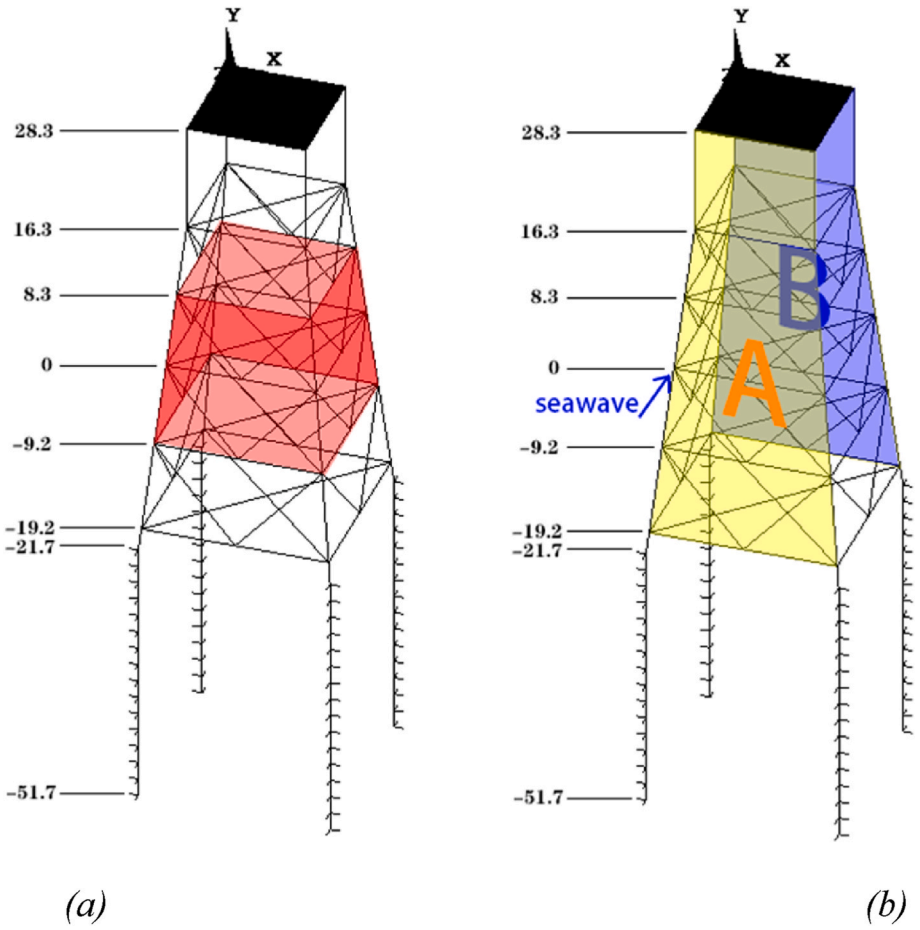

Fig. 1. (a) The 3D model of the fixed platform (unit: meter). (b) Rear (A) and front (B) surfaces.

4.1.1. Operating conditions

During the service of an offshore platform, its weight constantly varies as oil is extracted and transported. Therefore, the mass change is an important aspect of these structures. In this study, the added mass was numerically simulated by varying the density of the material in the work plane of the platform. The conditions considered in these case studies ranged from 800 kg/m^2 to 1000 kg/m^2 at 1 kg/m^2 intervals. Generally, in practice, the mass variations can be larger (for example, the Statfjord A platform in the North Sea has a storage capacity of 1.9 million barrels of oil ("Statfjord Field, North Sea," n.d.)), but choosing these conditions allows the evaluation of the accuracy of the methods, even with relatively small variations.

4.1.2. Damage conditions

To study the sensitivity of this damage detection method in this specific scenario, the structural elements located in the splash zone were considered as potential damage locations. As previously mentioned, these are shown in the red zone in Fig. 1 a. Damage was simulated by reducing the stiffness of these elements, and three levels of damage severity were considered: 25%, 50%, and 75%.

Although in general practice, an operational offshore platform should be repaired before reaching a sufficiently large loss in element stiffness, large reductions in stiffness (50% and 75%) were also considered because it is not certain that an element will be damaged slowly and progressively. An unexpected event can suddenly damage an element, causing it to suffer damage equivalent to a half or greater stiffness reduction, skipping the lightest damage step. In addition, severe damage can cause changes in the structural scheme and redistribution of loads, such that some vibration modes and their relative natural frequencies change unexpectedly in a nonprogressively monotonous manner. In a completely data-driven procedure, this could make identifying serious damage even more complicated than identifying minor damage.

In fact, the cointegration strategy to remove EOVs is based on the idea that these physiological effects cause variations in the frequency values without modifying their relationship; because it is considered legitimate to think that damage causes a local effect, which modifies each vibration mode differently, the damage detection occurs precisely by detecting these no longer coherent variations. For low damage levels, some frequencies may not be affected by variations, whereas others are. This could make the variation in their relationship more evident, making the damage more easily noticeable. For high damage levels, it is reasonable for each frequency to vary. This could confuse the algorithm and, paradoxically, make severe damage more difficult to detect than minor damage. Therefore, it seemed appropriate to test a broader spectrum of stiffness reduction, which certainly starts from minor damage (25%), but also includes very high values.

In addition, damage may occur at any time during the service. Therefore, to simulate the changing operating conditions of the platform, different deck weights (as previously described) were considered for each damage position and severity.

4.2. Force model

This study aimed to validate the proposed damage detection approach under realistic weather conditions. To this end, the JONSWAP and Davenport spectra were selected as the models for wave and wind forces, respectively.

In addition, as mentioned previously, the simulations (and analyses) were all performed in the time domain rather than in the frequency

domain, as is often the case for SHM approaches. This approach is used for the following reasons: First, from a technical perspective, the wave spectra differ at different depths. This means that a complex and computationally heavy analysis should be established, including many different wave force spectra and the use of specific software (because there is a limitation on the number of spectra in commercial FE software such as ANSYS). From a practical perspective, time-domain SHM is preferable because it does not require the use of the Fourier transform, which omits one step from the computations. Finally, from a conceptual standpoint, the time-domain analysis considers the transient and nonlinear effects of platforms that are lost in the frequency domain.

4.2.1. Wind force

Offshore design codes and guidelines provide several options for defining the expected wind loads. However, unlike structural design codes that focus on extreme loads and worst-case scenarios for design purposes, this study aims to test the effectiveness of the proposed damage detection method under regular conditions, which for dynamic identification is a precautionary choice (in fact, the less stressed a structure is, the less the modes are amplified, and the more difficult it will be to identify its modal parameters). Therefore, moderate wind conditions are used to validate the feasibility of the proposed method. The average wind velocity at 10 m above the sea surface was assumed to be 10 m/s. This value was taken from (Eidsvik, 1985) according to the histogram of the wind velocity reported in that study. However, to obtain the average velocity at each node, the wind profile must be considered. In this case, a logarithmic wind velocity profile was considered, as shown in Fig. 2 a. That is:

$$U(z) = u^* / k_a * \ln(z / z_0) \tag{21}$$

where k_a is the Von Karman's constant, equal to 0.4.

z is the height.

z_0 is the terrain roughness parameter.

u* is the friction velocity, defined as:

$$u^* = \sqrt{\kappa} \cdot U_{10} \tag{22}$$

where κ is a surface friction coefficient, defined as:

$$\kappa = k_a^2 \Big/ \left(ln(H/z_0)\right)^2 \tag{23}$$

where H is the reference height.

To simulate the fluctuating wind velocity, we employed the Davenport spectrum, which assumes constant wind turbulence across heights with a bias toward safety. The inverse fast Fourier transform (IFFT) was then used to transform the fluctuating wind velocity into the time domain.

The spectral density of the Davenport spectrum (Davenport, 1961) is expressed as follows:

$$S_D(f) = 2 \Big/ 3\,\sigma_U{}^2 \cdot (L_U/U_{10})^2 \cdot f \Big/ \left(1 + (f \cdot L_U/U_{10})^2\right)^{4/3} \tag{24}$$

where f is the frequency.

L_U is the length scale of the wind velocity process.

U_{10} is the 10-min average wind velocity.

σ_U is the standard deviation of wind velocity.

The corresponding wind pressure is expressed as follows and consolidated into the concentrated nodal force at each element intersection:

$$q_{wind} = 1/2\,\rho_{wind} |U+u|(U+u) \tag{25}$$

where ρ_{wind} is the air density, equal to 1.226 kg/m3.

U is the average wind velocity.

u is the fluctuating wind velocity.

4.2.2. Wave force

For simplicity, the waves were assumed to be completely generated by the wind. For moderate wind conditions such as those described in Section 4.2.1, the JONSWAP spectrum proposed in the Joint North Sea Wave Project is recommended (DNV GL, 2017). This can be defined as described in the original paper, as follows (Hasselmann et al., 1973):

$$S_J(\omega) = 5/16\ A_\gamma \cdot \frac{H_s^2 \omega_p^4}{\omega^5} \cdot e^{\left(-\frac{5}{4}\left(\frac{\omega}{\omega p}\right)^{-4}\right)} \cdot \gamma^{\exp\left(-0.5\left(\frac{\omega-\omega_p}{\sigma\omega_p}\right)^2\right)}. \tag{26}$$

where H_s: significant wave height.

ω_p: angular spectral peak frequency.

$A_\gamma = 1 - 0.287\ ln\,\gamma$: a normalizing factor.

σ: the spectral width parameter.

γ: the nondimensional peak shape parameter.

In this study, it is assumed that waves follow the linear wave theory, namely Airy's wave theory (Airy, 1849). Therefore, the wave velocity spectrum in the horizontal direction and the vertical direction can be respectively expressed as follows:

$$S_{vx/z}(\omega) = |\omega \cdot \cosh kz / \sinh kd|^2 S_\eta(\omega) \tag{27}$$

$$S_{vy}(\omega) = |\omega \cdot \sinh kz / \sinh kd|^2 S_\eta(\omega) \tag{28}$$

where d is the depth of the ocean.

z is the position of the point of action.

k is the wave number, $k = 2\pi/\lambda$, λ is the wavelength.

Because the formula varies with depth, the velocity spectrum changes point-to-point below the sea surface (see Fig. 3). To simplify the analysis, the depth of the sea was divided into several regions to use the

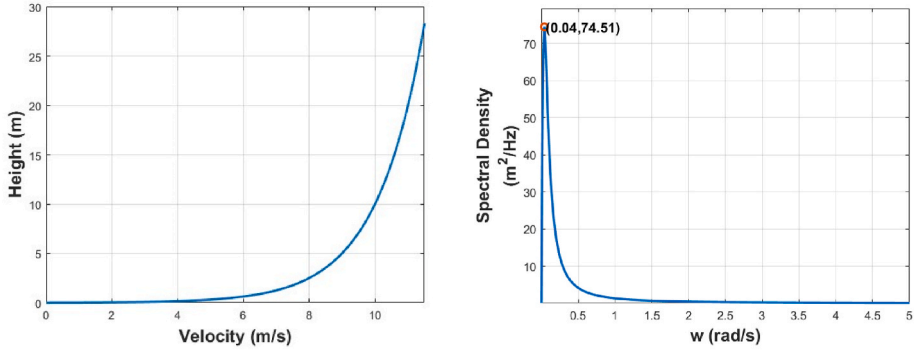

Fig. 2. (a) Wind velocity profile. (b) Davenport spectrum.

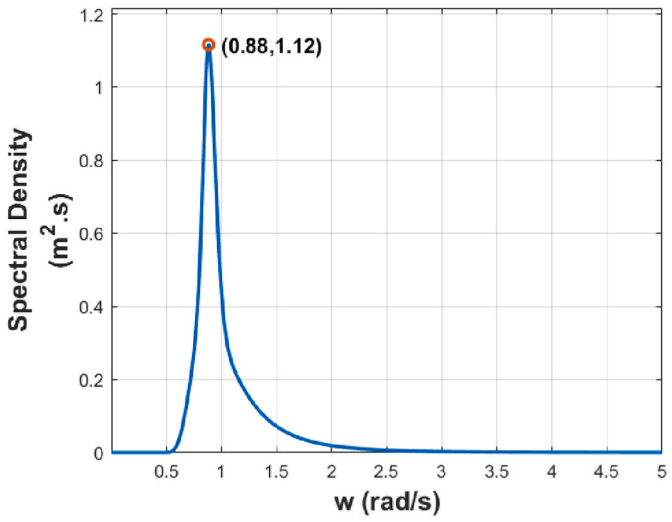

Fig. 3. JONSWAP spectrum.

velocity of the top points in a region to represent all the points within it. After obtaining the velocity spectrum at each point, an inverse fast Fourier transform (IFFT) is used to convert the frequency spectra into velocities in the time domain. In contrast to the velocity, the wave acceleration in the time domain was obtained from the direct gradient of the velocity rather than the acceleration spectra. This is because when using Airy's Wave Theory, acceleration and velocity are related to a phase difference. If the acceleration and velocity spectra are used simultaneously to obtain their respective time-domain data, information regarding the phase difference will be lost.

After the wave velocity and acceleration were obtained, the wave forces at different depths were derived. In the case studies, the considered platform had a relatively small size-to-wavelength ratio. Therefore, it did not disturb the motion of the waves. The Morison equation (Morison et al., 1950) can be used to calculate wave forces. Moreover, because this steel platform is fixed, the interaction between the platform and the external forces can be neglected. The wave forces of the vertical and horizontal elements are as follows:

$$f(z) = K_d v(t)|v(t)| + K_i a(t) \tag{29}$$

$$\text{where } K_d = 1/2\ C_D \rho D \tag{30}$$

$$K_i = (1 + C_A)\rho\pi D^2 \,/\, 4 \tag{31}$$

where C_D is the drag coefficient.

C_A is the added mass coefficient.

D is the diameter of the cross section.

ρ is the density of seawater.

This platform is supported by four legs, and the dimension of the pipe is small compared to the entire structure. Therefore, both rear (surface A in Fig. 1b) and front (B surface in Fig. 1b) side of the wave propagation direction is subjected to wave forces. The calculation method is always the same but with a phase difference. If the distance between the front and rear surfaces is L, the phase difference is

$$\Delta\theta = 2\pi L/\lambda \tag{32}$$

where λ is the wavelength.

The shadowing and interference effects caused by the diffraction of multiple legs are another factor when simulating the wave forces. The former applies to legs that are perpendicular to the wave propagation direction, and the wave forces in the middle leg are larger than those on the sides and those on a single leg under the same sea conditions. The latter is for legs that are parallel to the wave propagation direction. The forces on the front leg were greater than those on the rear leg. In this case, because the distance between the legs is sufficiently large compared to the diameter of the cross section, neither effect is considered.

5. Application of the damage detection procedure

Based on previously introduced theories, the effectiveness of the damage detection method in this specific scenario can be tested as follows: first, the procedure for generating numerical data is illustrated. Then, the damage detection procedure itself, based on the output-only identification of the natural frequencies (via FDD) and the generation of cointegration relationships, follows.

The first part, numerical data generation, was intended only to test the procedure. In this regard, steps ***I*** and ***II*** are required exclusively to generate a suitable database for validating the method for offshore structures. For actual SHM in practical applications, one will assume to depart from the recordings of the structure's dynamic response (captured by accelerometers or other sensing devices). Thus, the FDD (point ***a*** in the damage detection procedure) is applied directly to these acquired time histories.

Furthermore, for continuous monitoring, all steps (***a***–***g***) were applied only once and offline to set the "normality model," considering the time series selected from the offshore structure under normal operating conditions (i.e., without damage scenarios). Therefore, only steps ***h*** and ***i*** are performed online—that is, at regular intervals on the newly acquired time series—to assess whether they belong to the normality model. In the latter case, this can be used as a proxy for damage occurrence since the previous check.

5.1. Numerical data generation

I. Numerical simulations were performed under different operating and damage conditions to simulate the changing deck mass and damage development following the sequence of increasing damage severity, that is, undamaged, 25%, 50%, and 75%, and the time-domain acceleration data were extracted from the FE method.

II. The time series of the simulated loading and unloading was created by concatenating several *tests.* Each test was used to identify the structure dynamically. *Test numbers,* on the abscissa of the graphs shown below, represent the corresponding progressive numbers.

5.2. Damage detection procedure

a. Apply FDD to identify the natural frequencies of each test considered in ***II.***
b. Select a specific range in the time series (frequency and mass data) from the undamaged conditions.
c. Apply the ADF test to these time series ranges to check their order of integration.
d. Extract the time series that have the same order of integration.
e. Choose one natural frequency for the ML regression model and the other data as inputs (predictors).
f. Obtain a possible cointegration relationship, which is considered a damage indicator, by calculating the ML model residual as the difference between the observed and predicted data.
g. Apply the ADF test to the residuals to verify the validity of the established cointegration relationships.
h. Use the trained ML models to predict the selected natural frequency by relying on data unknown to the ML algorithms (both unseen undamaged and damaged conditions).
i. Calculate the model residual series and their stationarity and evaluate their trend in a control chart.

6. Results

The intermediate and final results reported in this section were

obtained by implementing the methodology described in the previous sections using MATLAB R2022b.

6.1. Natural frequency identification

For natural frequency identification, a consistent procedure was followed for all conditions. Time-domain acceleration data were collected from 40 nodes over 100 s.

Fig. 4 presents the acceleration data in three directions for the node highlighted in red, reflecting the scenario of an undamaged platform with a work plane density of 800 kg/m^2.

Applying the FDD method (Brincker et al., 2001) yielded singular values for the spectral density function. Natural frequencies were identified by selecting the peak values.

By utilizing FDD on many acceleration signals (derived from different mass conditions of the structure) and connecting the identification results, a frequency time series was obtained for each vibration mode. Some of these can be chosen for cointegration analysis. As long as the first natural frequency selected is greater than 1 Hz, the natural frequency identification process remains unaffected by the wind and wave force frequencies, whose peaks are considerably lower than 1 Hz.

The subset of natural frequencies involved in the cointegration analysis should be selected based on their sensitivity to the expected damage and/or mass variations in the defined mass range. Specifically, the selected modes are the first flexural mode along Z (i.e., in the wave impact direction) at around 1.09 Hz (taking the intact platform with a mass of 800 kg/m^2 distributed on the deck as reference), the second flexural mode along X (i.e., orthogonal to the wave load) at around 1.91 Hz, the first torsional mode at around 2.05 Hz, and a mixed torsional-flexural mode along X at around 2.83 Hz. The results are shown in Fig. 5. The selection criteria were to use global modes that could involve a large portion of the structure, thus avoiding local modes (especially deck modes, which were found even at relatively low frequencies below 1.3 Hz), omitting vertical or mostly vertical modes, and avoiding the use of closely spaced modes, for example the flexural modes along X and Z, which are very close owing to the symmetry of the structures. The latter were found to be more difficult to isolate properly with the FDD procedure, and thus returned less reliable results.

6.2. Simulation of concatenated time series

The simulated time series of the mass distributed at the work plane, which is responsible for physiological variations in natural frequencies (i.e., harmlessly caused by variations in operating conditions rather than damage), is shown in Fig. 6. For each damage severity (from 0% to 75%), two filling and draining rounds were considered. In the first round, the density changed from 800 kg/m^2 to 1000 kg/m^2 and back to 800 kg/m^2, whereas the maximum density in the second round was 900 kg/m^2.

The speed of the filling process was assumed to be five times slower than that of the drainage process. This is based on the guidelines recommended by the Norwegian Oil and Gas Operations Committee (Norwegian Oil and Gas Association, 2015) followed by all the main companies involved in offshore extraction from the Norwegian Continental Shelf including BP, Statoil, Shell, Eni, and Total. For example, consider the Heidrun combined production and drilling platform, which operates in the same area and has declared a current production of 60,000 barrels and 250,000 barrels during its peak period ("Heidrun—oil and gas field in the Norwegian Sea—Equinor," n.d.). On average, these translate to circa 400 m^3/h and 1650 m^3/h, respectively. The oil is exported via a permanently moored floating storage vessel (Heidrun B FSU) to tankers and shipped to the market. To reduce risk exposure, the aforementioned guidelines require the loading rate (performed through a bow-loading system) to be set according to the total cargo tank capacity. Even for the smallest tankers, this value was never lower than 3000 m^3/h. Thus, even for the same platform, the loading/unloading speed ratio could oscillate between $\sim$ 2 and 7.5 times slower, depending on both the platform's production capabilities and tanker cargo size; 5 was assumed as the middle point.

Three damage conditions and one undamaged condition, considering the reduction in the stiffness of the elements in the splash zone, were arranged according to the damage severity to simulate real structural damage.

At this point, the natural frequencies corresponding to all the mass and damage severity conditions were obtained. In particular, 1800 observations were obtained and concatenated to yield a time series of the four natural frequencies ordered consistently with mass variation. Moreover, to fully simulate the data extraction in practice, various

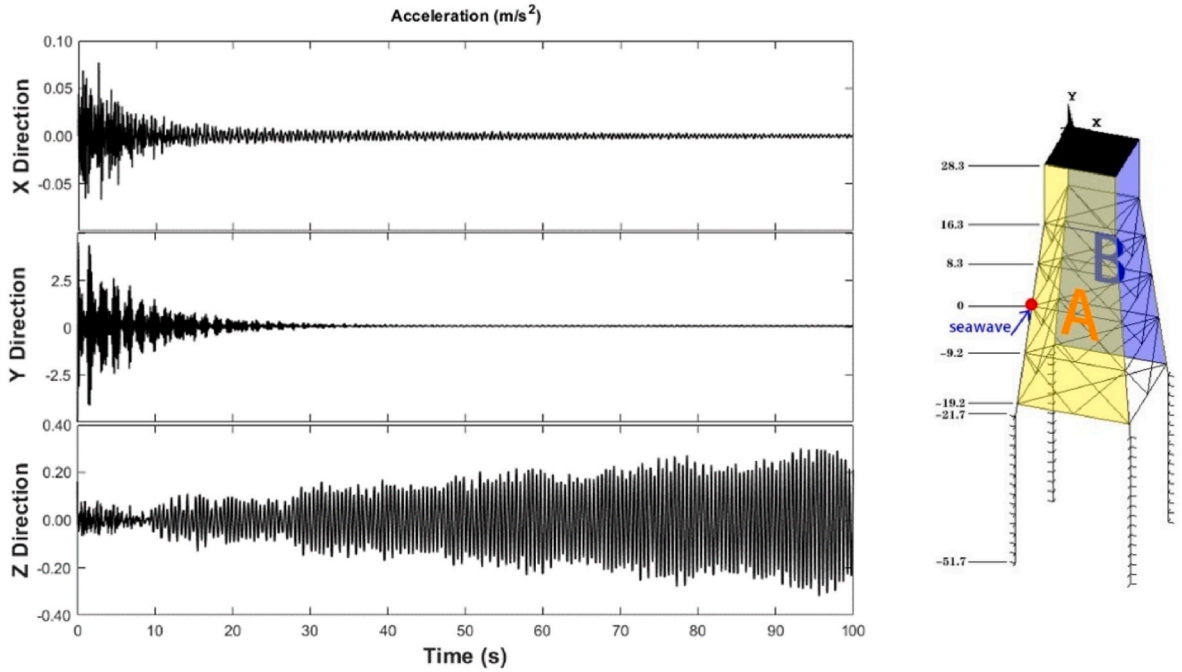

Fig. 4. Acceleration data in three directions (parallel to the x-, y-, and z-axes). (Please note the different scales for the accelerations along the three directions.)

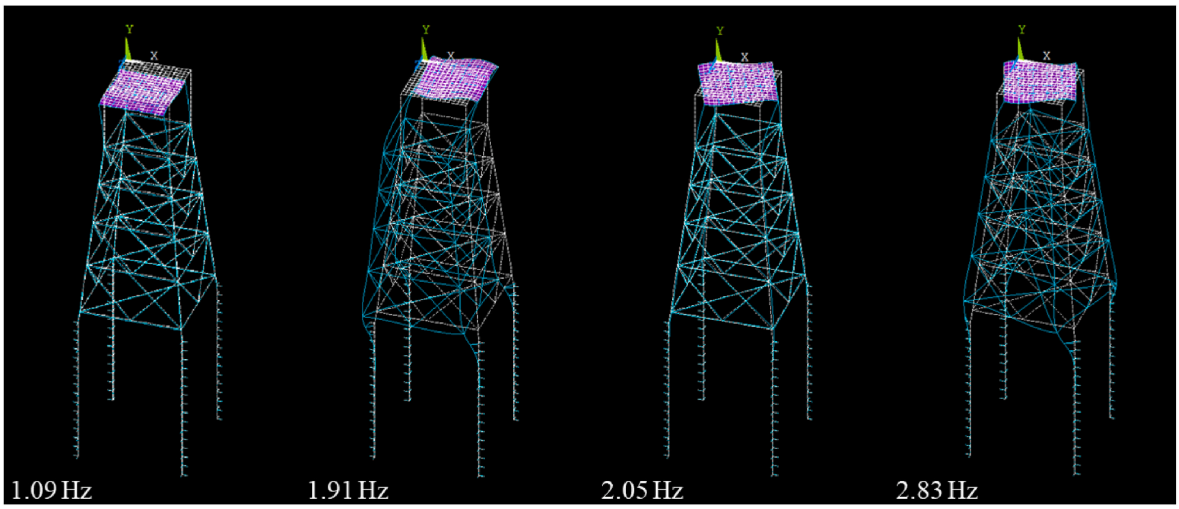

Fig. 5. Selected modes.

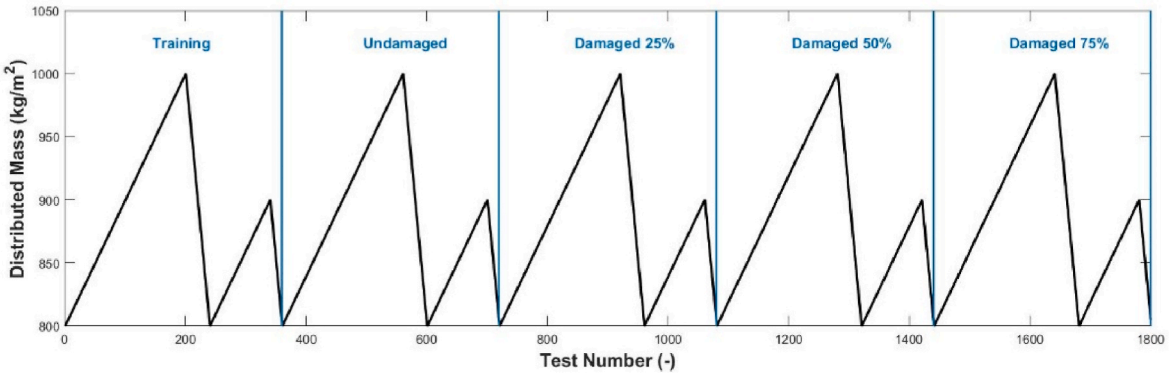

Fig. 6. Mass time series.

amounts of artificially generated WGN were added to all time series according to the following common formulation:

$$y_{meas} = y_{true} + \sigma_n \text{rand} \tag{33}$$

Where: y_{meas} is the simulated "measured" (noisy) signal.

y_{true} is the simulated "true" (noise-free) signal.

σ_n is the arbitrary standard deviation of the added noise.

rand is a random scalar drawn from the standard normal distribution.

Here, taking $\sigma_n = \sigma/5$, i.e., one fifth of the signal standard deviation as an example, the first natural frequency time series is obtained as shown in Fig. 7.

6.3. ADF tests

After obtaining all the time series, a set of observations for the subsequent training of the ML algorithms was selected, and ADF tests were applied to determine the order of integration at a 95% confidence level. The results show an order of integration equal to one for all natural frequency time series. The training time series of the mass was also tested using ADF in preparation for later use. Because its order of integration is the same as that of the natural frequencies used, the set of mass

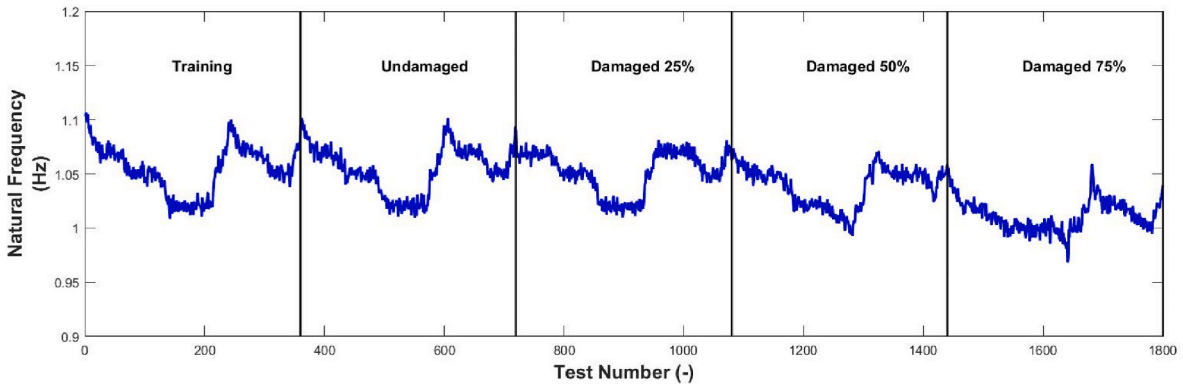

Fig. 7. Time series of the first natural frequency with 1/5 standard deviation noise.

time series can also be included in the inputs, with the aim of making the regression model more accurate. The results of the ADF tests for the four natural frequency time series, each subjected to a 1/5 standard deviation noise, are presented in Table 1.

6.4. Results based on SVM regression

The cointegration relationship, that is, the residual of a regression model in this case, also depends on the ML regressor and its tuning. In this case study, although the residuals of the training tests provided by linear regression are stationary, the predictions and observations of the training outputs deviate significantly, indicating that linear regression is not sufficient. Therefore, nonlinear cointegration with the Gaussian kernel function used in the regression model was used in these case studies.

6.4.1. Regression model based exclusively on natural frequencies as inputs

First, only sets of natural frequencies were considered for applying nonlinear cointegration analysis based on the SVM. Four natural frequencies were used in this analysis, one of which was chosen as the regression target. Thus, there are four different types of regression models for each case: $f_1^{'} = F(f_2,f_3,f_4)$, $f_2^{'} = F(f_1,f_3,f_4)$, $f_3^{'} = F(f_1,f_2,f_4)$, and $f_4^{'} = F(f_1,f_2,f_3)$. Although, in theory, all four models could be used to predict the structural behavior, here, the first one, $f_1^{'} = F(f_2,f_3,f_4)$, is chosen because the first natural frequency is considerably sensitive to mass change, and the first mode is expected to be among the most sensitive to the effects of the specific simulated damage. After regression, the residuals of the training observations were fed into the ADF test (confidence level: 95%) and found to be stationary, proving to be valid candidates for the anomaly detection procedure.

The relationship established based on the SVM is used to predict the first natural frequency over time. The results for different noise levels are shown in Figs. 8–10. Each figure shows the original values of the natural frequencies (gray lines). The corresponding values predicted by SVM regression are reported with orange lines and represent the single set seen by the algorithm in the training phase in undamaged conditions. After the first 360 observations (used for the training dataset), several test sets in which the severity of damage increased are reported: blue lines (0% damage severity, undamaged), green lines (25% damage severity), dark blue lines (50% damage severity), and light blue lines (75% damage severity). All sets included 360 observations. The results provide the residuals of each test in an X-chart and a type of control chart from Statistical Process Control (SPC) (Gaudard and Ramsey, 1997) with associated upper and lower control limits (UCL and LCL, respectively). Vertical lines were drawn to separate the different conditions corresponding to the increasing damage intensity.

Figs. 8–10 show that the regression model targeted for the first natural frequency can successfully predict the damage in high-damage-intensity conditions. However, as the amount of artificially added signal noise increases, the predictive ability decreases significantly. When adding noise with an amplitude equal to 1/3 of the signal standard deviation, the UCL and LCL sets on the training set were so wide that they contained fluctuations based on damage severity of 50%. This translates into a failure to detect the damage, although residuals moving from the average of the training tests may still be considered warning signals.

Table 1
ADF tests.

No. Of Frequency (−)	ADF Statistic (−)	Critical Value (−)	Stationarity	Order of Cointegration (−)
First Frequency	−0.1630	−1.9415	N	1
Difference of First Frequency	−30.2517		Y	
Second Frequency	−0.0341		N	1
Difference of Second Frequency	−34.3720		Y	
Third Frequency	0.0552		N	1
Difference of Third Frequency	−31.7670		Y	
Fourth Frequency	−0.1074		N	1
Difference of Fourth Frequency	−31.9278		Y	

6.4.2. Regression model based on both natural frequencies and mass distributed as inputs

Section 6.3 discussed the proof that the mass time series had the same order of integration as the natural frequencies used. Therefore, a mass time series can be considered a set of inputs. A new regression model is defined, with the first natural frequency as the target and other frequencies together with the time-varying mass M at the work plane as inputs, which can be denoted as $f_1^{'} = F(M, f_2, f_3, f_4)$.

After nonlinear ML regression analysis, the residuals of the training tests for each σ_n assumed, are taken into ADF tests (confidence level: 95%), and they are all stationary. Thus, cointegration was successfully established. These relationships were used to predict the first natural frequency time series. The results are shown in Figs. 11–13.

As expected, including the mass time series as one of the inputs increased the accuracy of damage prediction. First, for all these noise conditions, the residuals can be used to predict the damage case with a 75% reduced stiffness, because it consistently exceeds the UCL, whereas this is not the case for the natural frequencies alone in the noisier cases (Figs. 9 and 10), where a slight departure is found. Second, as shown in Table 2, the widths between the upper and lower control lines are smaller than before, indicating that a more accurate regression or cointegration relationship is established.

6.5. Results based on the RVM

The cointegration relationship generated based on the RVM follows the same procedure as that based on the SVM. Inputs with exclusively natural frequencies and those with natural frequencies and mass are described in this section and are denoted as $f_1^{'} = F(f_2, f_3, f_4)$ and $f_1^{'} = F(M, f_2, f_3, f_4)$. The results are shown in Figs. 14–16 (inputs: natural frequencies) and Figs. 17–19 (inputs: natural frequencies and masses).

6.5.1. Regression model based exclusively on natural frequencies as inputs

The RVM provides a faster analysis speed than the SVM. Nevertheless, there are no substantial differences in terms of accuracy. Using the residuals shifting from the mean of the training tests as an indicator of the damage condition, the magnitude of this shift is not more pronounced in RVM than in SVM. This was visible for all noise conditions, with low (Figs. 8 and 14), medium (Figs. 9 and 15), and high levels of artificially added noise (Figs. 10 and 16).

6.5.2. Regression model based on both natural frequencies and mass distributed as inputs

Finally, the inclusion of the mass time series enabled the RVM to improve the regression model. This improvement is in line with that achieved with the SVM, that is, the enhancement shown in Fig. 17 with respect to Fig. 14 is comparable to that shown in Fig. 11 with respect to Fig. 8. Hence, as stated before, adding the time series of mass changes into the cointegration process produced higher accuracy in the regression model, and resulted in a tighter UCL and LCL (calculated as a function of the standard deviation of the residual in the training set), and therefore, a greater ability to capture even smaller anomalies. However,

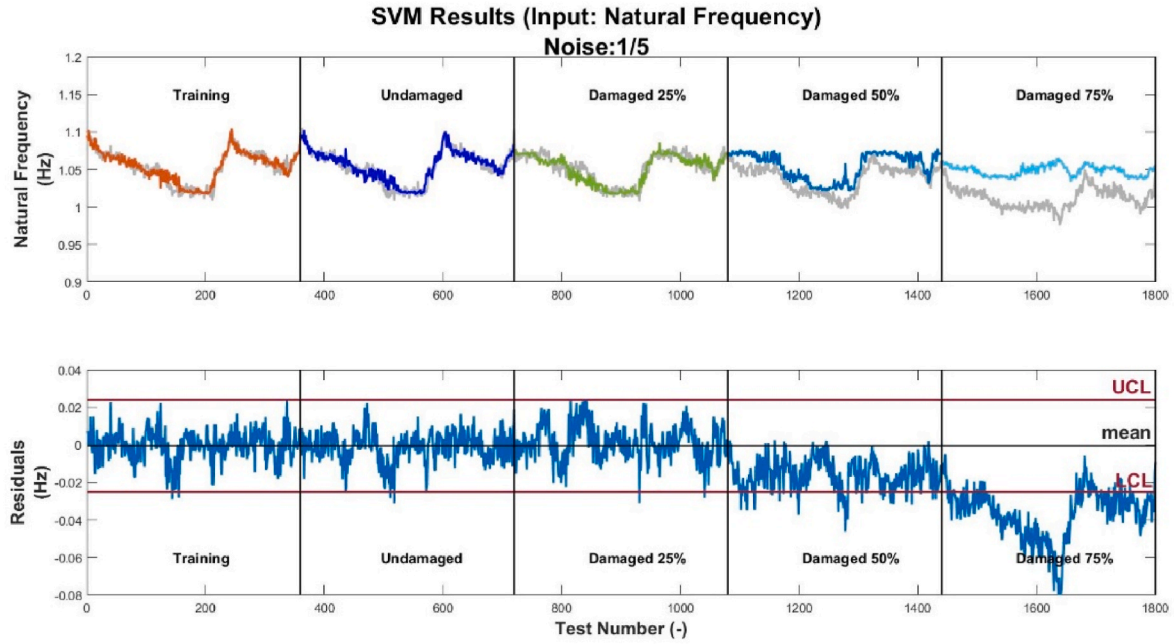

Fig. 8. SVM results with 1/5 standard deviation noise (input: natural frequency).

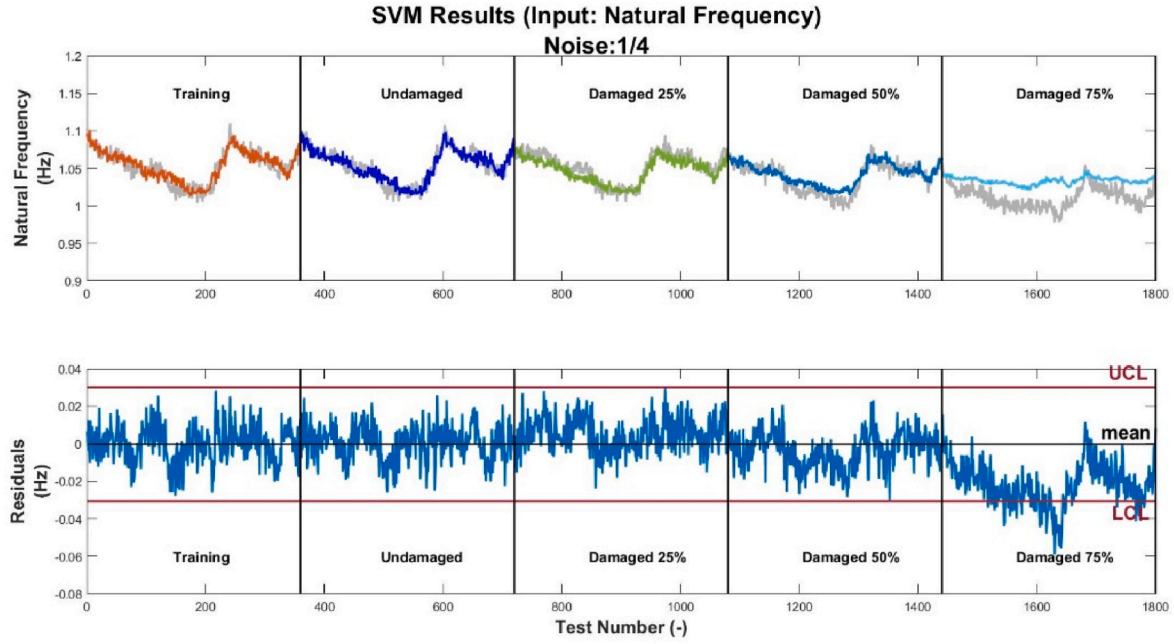

Fig. 9. SVM results with 1/4 standard deviation noise (input: natural frequency).

except for faster computation, the use of the RVM over the SVM did not significantly improve the damage-detection capabilities of the method.

Table 3 summarizes the widths between control lines for different inputs and noise levels.

7. Discussion

Based on several scenarios, it has been proven that the anomaly-detection procedure derived from cointegration, ML regression, and the X-chart could be a valuable tool for monitoring the structural conditions of offshore platforms exposed to wind and wave loads. In addition, the following conclusions were drawn.

i. Natural frequency identification was vital for this analysis, particularly for platforms with similar modes. For this platform, FDD was applied to extract only four selected global modes, although various local and close modes exist (the former at higher frequencies and the latter because of its symmetric structure). If one is interested in monitoring higher natural frequencies and/or close modes, other output-only identification methods can be considered. However, this can be achieved with higher computational cost and complexity. In this study, damage detection based on global flexural and torsional modes was successfully achieved. Therefore, obtaining the dominant natural frequencies from the FDD proved to be effective and computationally convenient.

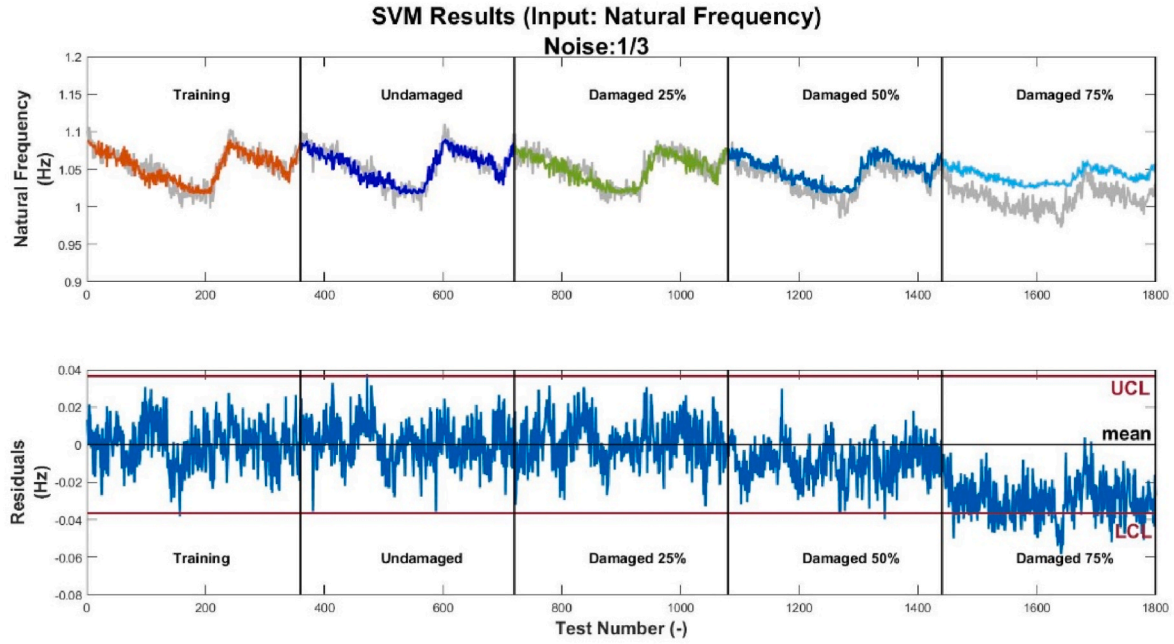

Fig. 10. SVM results with 1/3 standard deviation noise (input: natural frequency).

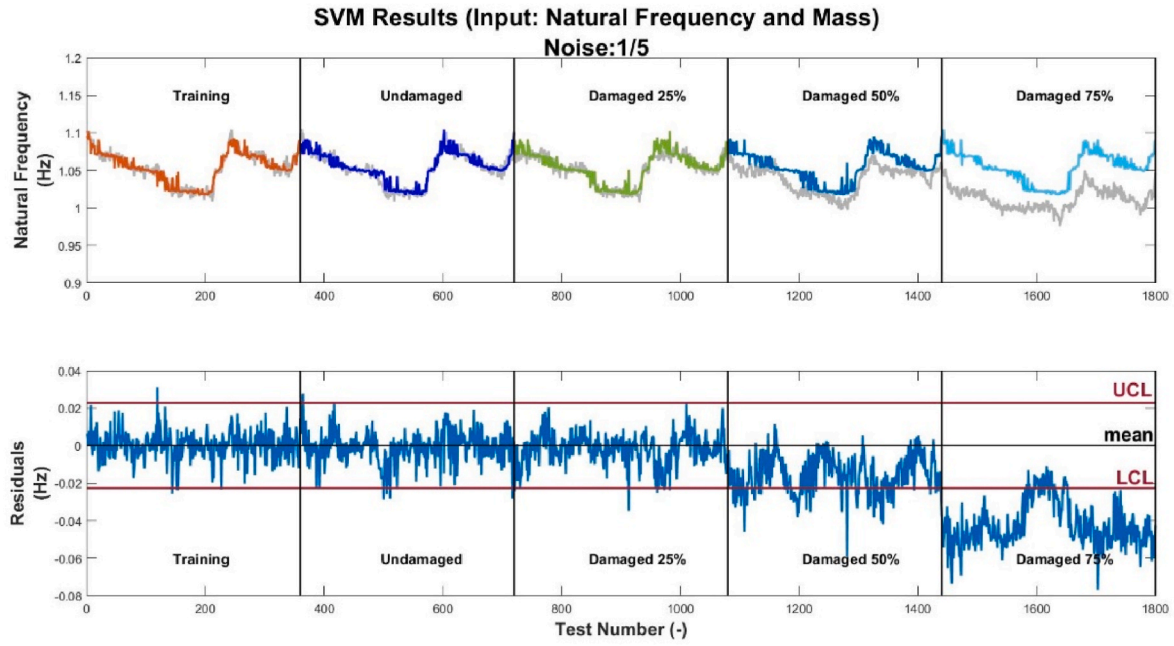

Fig. 11. SVM results with 1/5 standard deviation noise (input: natural frequency and mass).

ii. In particularly unfortunate cases from the SHM perspective, frequency variations due to structural damage could be very slight or very similar in various modes, and a regression model based on frequency data alone cannot predict the target frequency well, even in the undamaged case. This implies a minimum residual of the model that may fail to cross the thresholds and is therefore difficult to identify. Therefore, simply using natural frequencies to build a cointegration relationship may not be reliable. In SHM, the anomaly detection process can be enriched by additional related dynamic time series that are not affected by damage, such as mass (as reported in this paper) or temperature (as in many other literature cases). Because most offshore platforms are used for oil extraction, mass monitoring is a daily task. In this case, using both natural frequency and mass changes helps build a more complete and accurate damage detection system. Simultaneously, the additional cost (in terms of additional sensors) was relatively low. Therefore, using a combination of nonhomogeneous, related dynamic data for damage detection was found to be an optimal strategy.

iii. In this study, a cointegration relationship based on SVM and RVM was generated. For both the SVM and RVM, when the residuals shift sharply from the mean value and/or exceed the set control limits, one can conclude that the platform is experiencing abnormal behavior, which may be due to damage. Compared to the SVM, in this specific application, the RVM provided a more

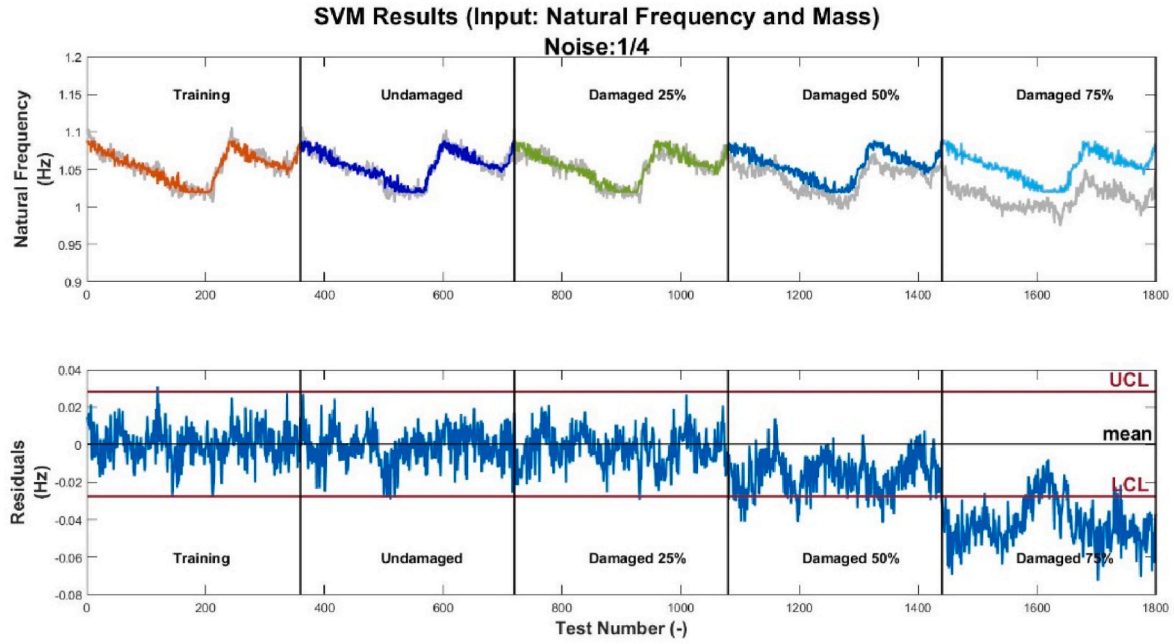

Fig. 12. SVM results with 1/4 standard deviation noise (input: natural frequency and mass).

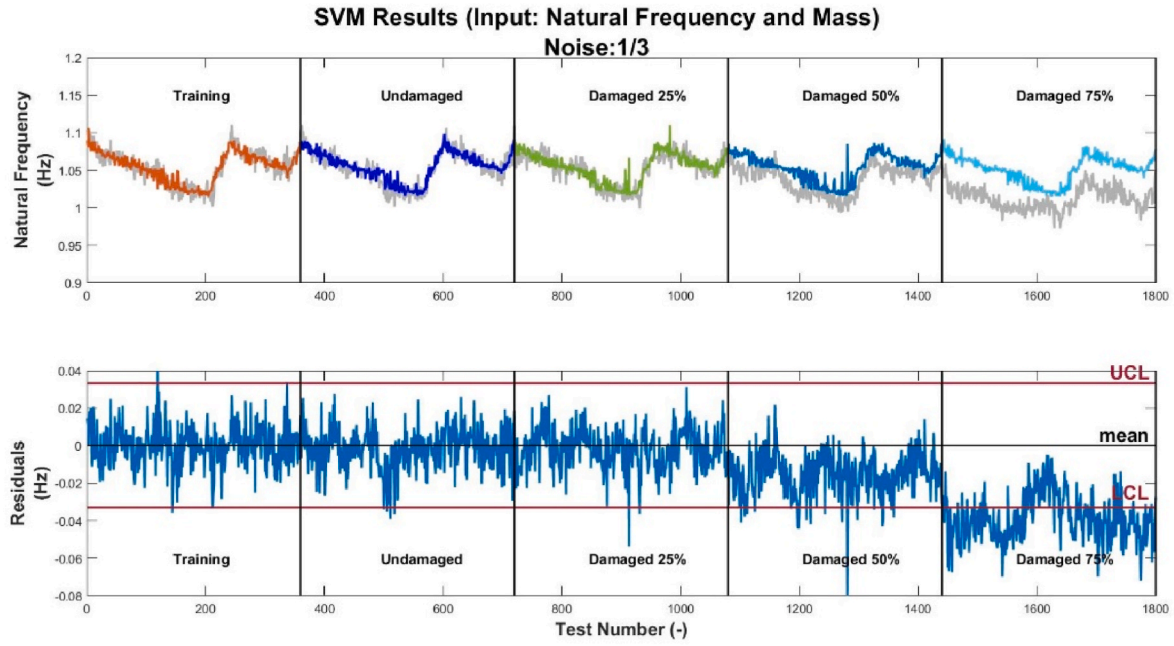

Fig. 13. SVM results with 1/3 standard deviation noise (input: natural frequency and mass).

Table 2
Widths between control lines.

Inputs	Noise levels in the time series		
	$\sigma_n = \sigma/5$	$\sigma_n = \sigma/4$	$\sigma_n = \sigma/3$
Natural Frequency	0.049	0.061	0.074
Natural Frequency + Mass	0.046	0.056	0.066

efficient and faster detection method, but no significant improvements in terms of accuracy.

iv. In the various proposed cases, by increasing the noise level (which, in reality, would correspond to a less accurate dynamic identification phase), the ability to identify damage decreases. Therefore, to enhance the sensitivity of this strategy for damage monitoring in future research, efforts should be made to reduce the influence of noise; for example, by improving the dynamic identification accuracy and/or optimizing the sensor layout.

v. Finally, it is important to remember that this case study assumes that the influences of external factors, such as marine growth and seabed movement, are negligible. Nevertheless, these external factors may affect the effectiveness of the damage detection method. For example, marine growth increases the mass of platforms, thus affecting their natural frequencies. In addition, from Equations (29)–(31), it can be seen that the wave forces are

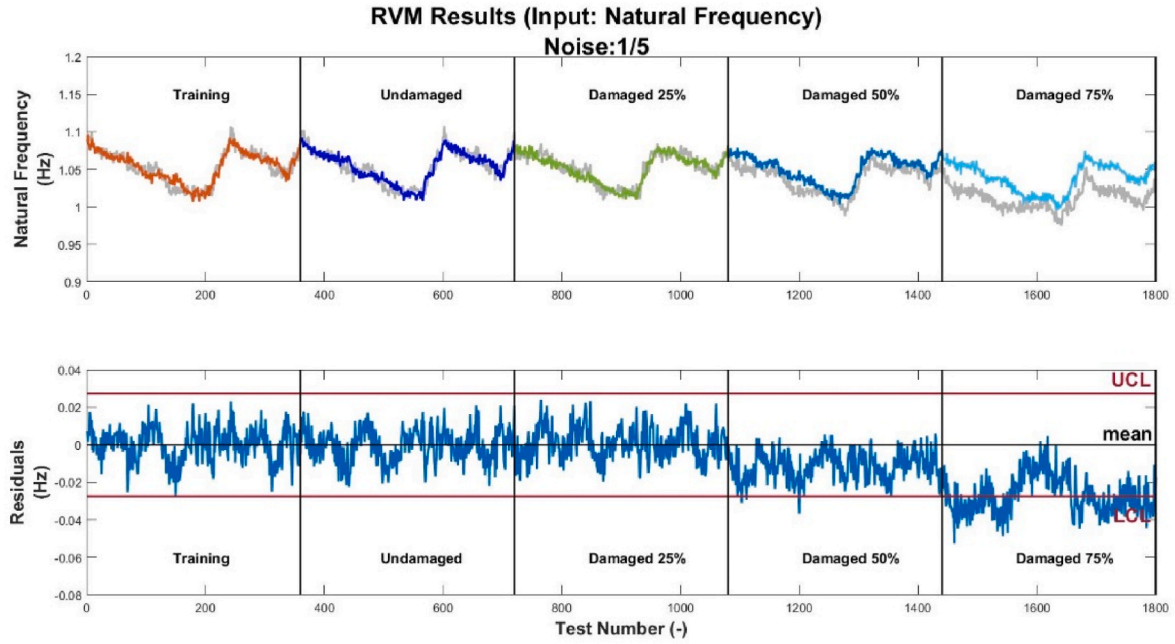

Fig. 14. RVM results with 1/5 standard deviation noise (input: natural frequency).

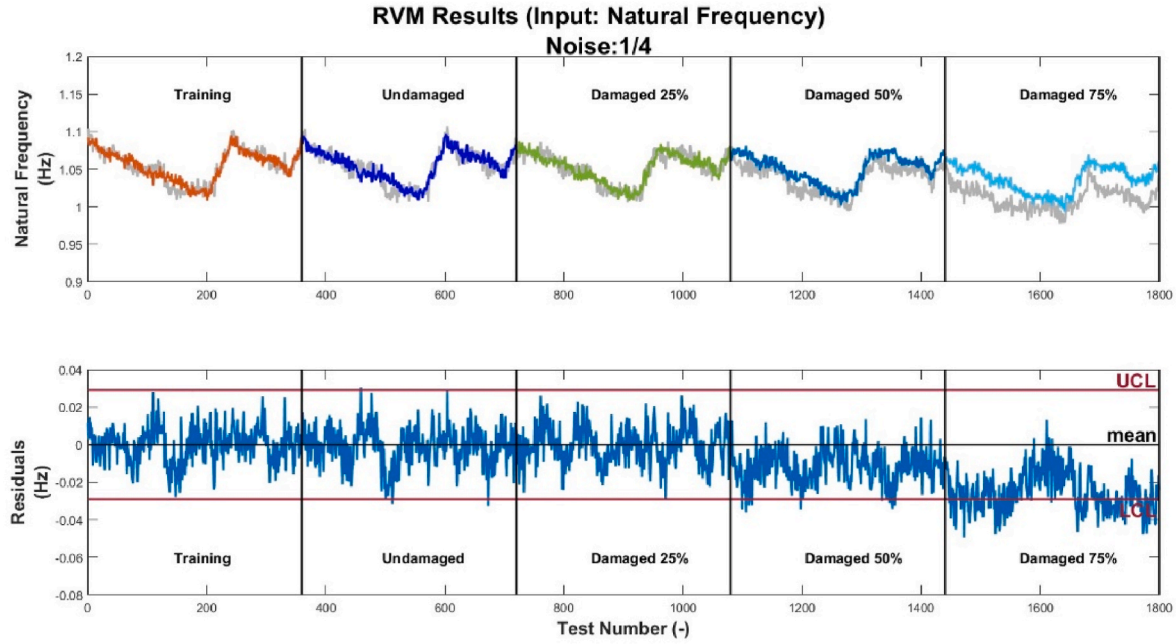

Fig. 15. RVM results with 1/4 standard deviation noise (input: natural frequency).

related to the cross section of the elements, and marine growth might increase the diameter.

8. Conclusions

This paper discusses the application of a damage-detection approach to offshore structures based on their evolving dynamic features. Specifically, to the best of the authors' knowledge, the strategy described here represents both the first application of output-only cointegration-based SHM to offshore platforms, and the first instance of cointegration applied to a time series that reflects a combination of natural frequency and mass change.

Compared to previous applications on bridges and buildings, this study addresses some specific aspects of offshore structures related to both external wind and wave forces and related dynamic parameters given as inputs to the algorithm, that is, the variable mass of the extracted fluid. The rationale is quite simple in its core concepts. By training a model to predict the value of a selected natural frequency, given a set of other natural frequencies and a time-changing mass distribution, a cointegration relationship can be established based on undamaged training conditions. This relationship can then be used to predict the natural frequency of the target under unknown conditions. If the predicted values are close to those observed, the platform's dynamic behavior is unaltered; otherwise, a statistically relevant structural change occurs. Because structural changes unrelated to damage (such as mass variations) were already included in the model, the detected

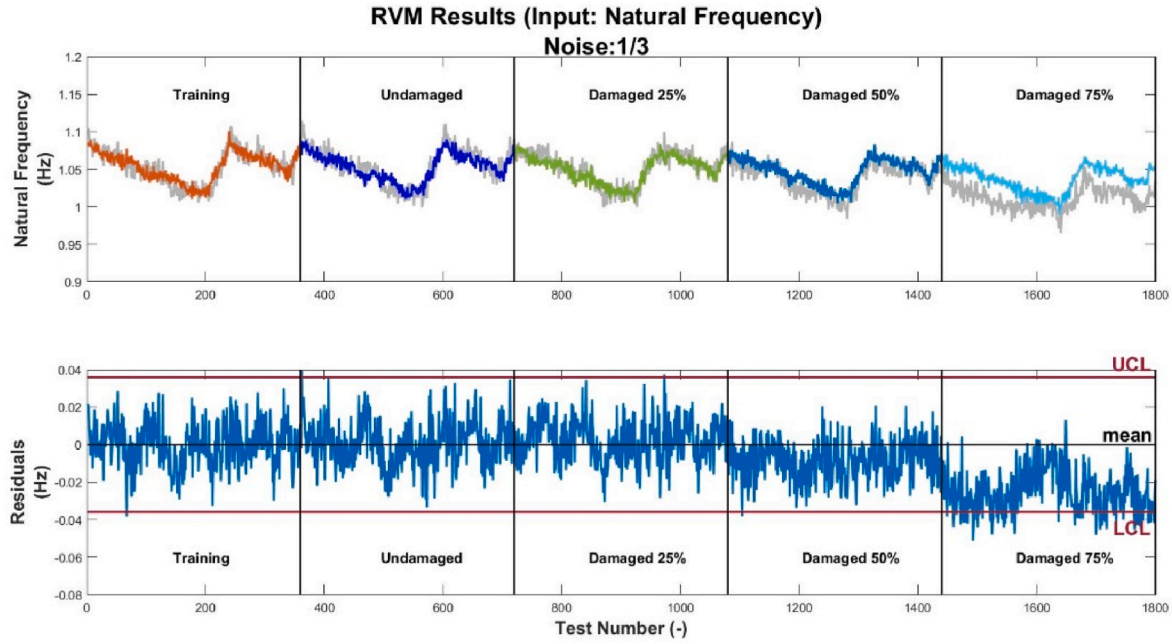

Fig. 16. RVM results with 1/3 standard deviation noise (input: natural frequency).

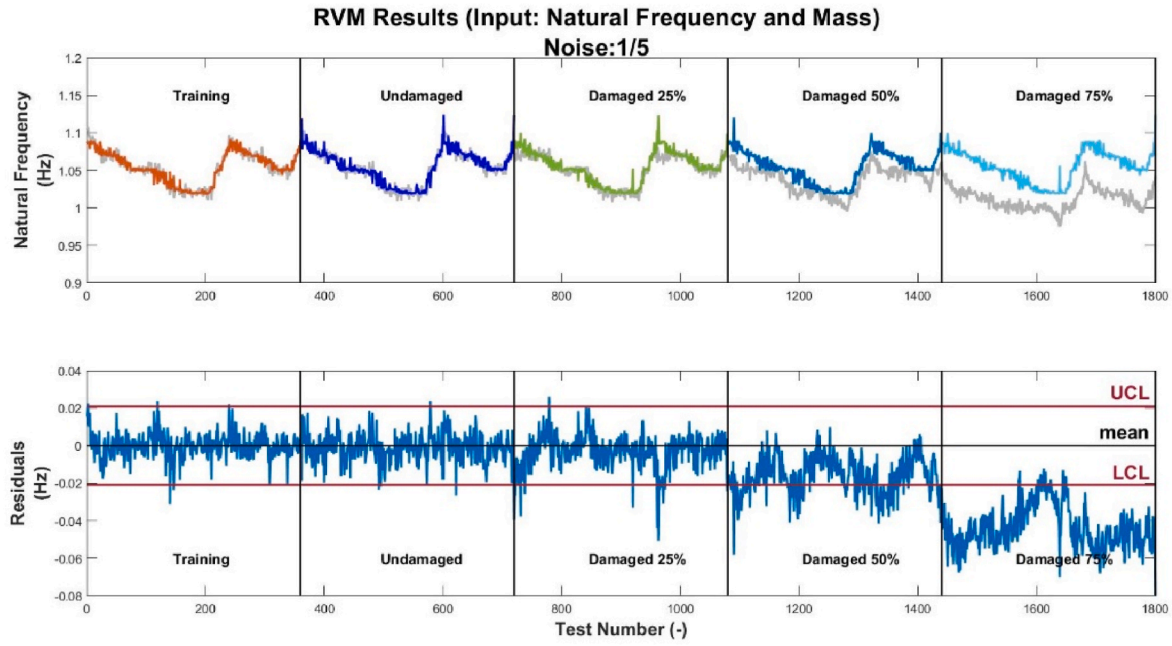

Fig. 17. RVM results with 1/5 standard deviation noise (input: natural frequency and mass).

anomaly was likely induced by the occurrence and development of damage.

To implement the proposed algorithm in detail, the FDD was used to extract the natural frequencies from the acceleration data obtained from the in-service platform. The natural frequency, estimated over a period when the platform was known to be undamaged, was considered the dynamic characteristic indicator. Considering different sets of natural frequency time series together with their corresponding mass time series, the ADF test was applied to obtain their respective orders of integration. By choosing appropriate datasets, a cointegration relationship can be determined using the SVM or RVM regression. The latter has been found to be more effective in computational terms, but not significantly better in terms of accuracy.

In conclusion, this study proves that the applied damage detection approach is effective for offshore platforms that are exposed to realistic wind and wave loads and suffer moderate to severe damage. Future research could aim to improve detection sensitivity, for example, through noise reduction or by focusing on defining damage thresholds more in line with the case study, such as those that evolve and taper over time.

Funding

This research did not receive any specific grant from funding agencies in the public, commercial, or not-for-profit sectors.

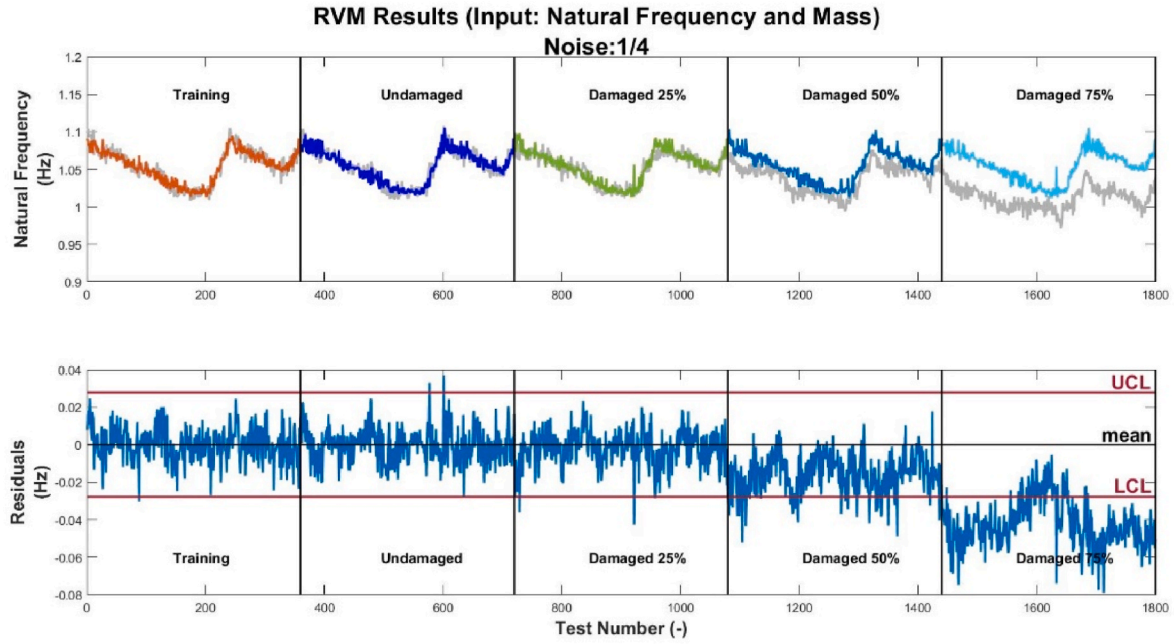

Fig. 18. RVM results with 1/4 standard deviation noise (input: natural frequency and mass).

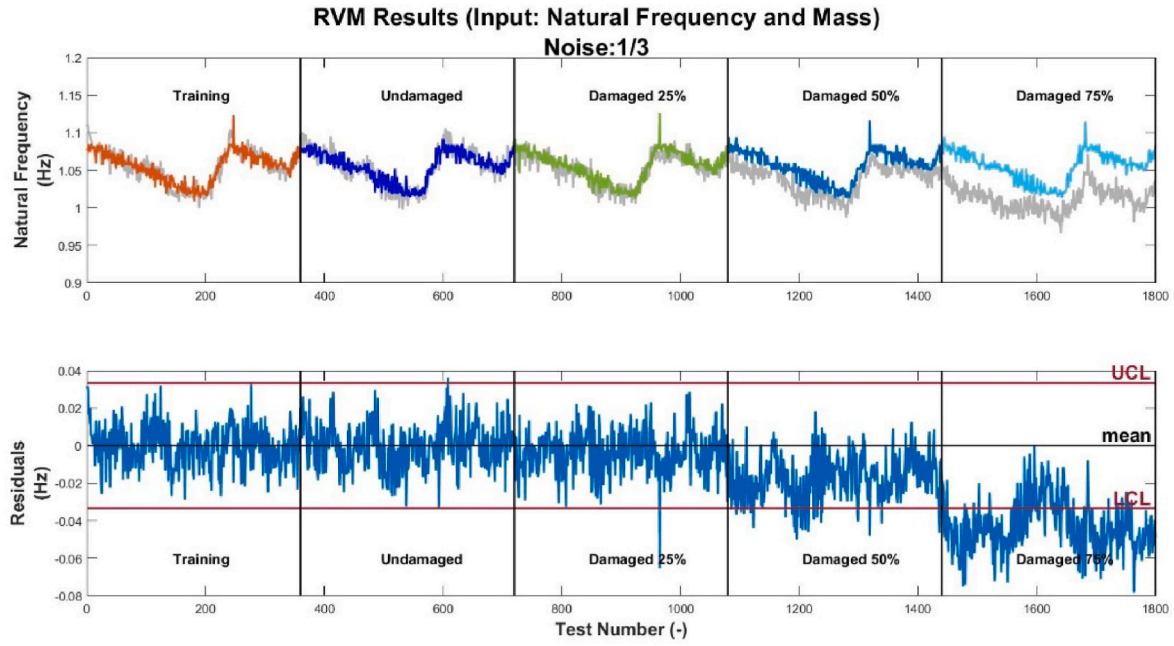

Fig. 19. RVM results with 1/3 standard deviation noise (input: natural frequency and mass).

Table 3
Widths between control lines.

Inputs	Noise levels in the time series		
	$\sigma_n = \sigma/5$	$\sigma_n = \sigma/4$	$\sigma_n = \sigma/3$
Natural Frequency	0.054	0.058	0.072
Natural Frequency + Mass	0.042	0.056	0.066

CRediT authorship contribution statement

H. Kuai: Writing – original draft, Software, Methodology, Formal analysis. **M. Civera:** Writing – review & editing, Visualization, Software, Methodology, Conceptualization. **G. Coletta:** Writing – review & editing, Software, Methodology, Conceptualization. **B. Chiaia:** Writing – review & editing, Supervision. **C. Surace:** Writing – review & editing, Supervision, Resources, Project administration, Conceptualization.

Declaration of competing interest

The authors declare that they have no known competing financial interests or personal relationships that could have appeared to influence the work reported in this paper.

Data availability

Data will be made available on request.

Acknowledgments

The Authors would like to thank Mr. Hammoud Raed for his precious help in the early stages of this research work. This work is part of the research activity developed by the authors within the framework of the "PNRR": SPOKE 7 "CCAM, Connected Networks and Smart Infrastructure" - WP4.

References

Airy, G.B., 1849. Tides and Waves. J.J. Griffin, London.
Almar-Naess, A., Haagensen, P.J., Lian, B., Moan, T., Simonsen, T., 1984. Investigation of the Alexander L. Kielland failure-metallurgical and fracture analysis. J. Energy Resour. Technol., Transac. ASME 106. https://doi.org/10.1115/1.3231014.
Brincker, R., 2014. Some elements of operational modal analysis. Shock Vib. 2014 https://doi.org/10.1155/2014/325839.
Brincker, R., Zhang, L., Andersen, P., 2001. Modal identification of output-only systems using frequency domain decomposition. Smart Mater. Struct. 10, 441–445. https://doi.org/10.1088/0964-1726/10/3/303.
Chen, H.-P., Ni, Y.-Q., 2018. Introduction to structural health monitoring. In: Structural Health Monitoring of Large Civil Engineering Structures. https://doi.org/10.1002/9781119166641.ch1.
Civera, M., Surace, C., 2022a. Non-destructive techniques for the condition and structural health monitoring of wind turbines: a literature review of the last 20 years. Sensors. https://doi.org/10.3390/s22041627.
Civera, M., Surace, C., 2022b. Instantaneous spectral entropy: an application for the online monitoring of multi-storey frame structures. Buildings 12. https://doi.org/10.3390/buildings12030310.
Civera, M., Zanotti Fragonara, L., Surace, C., 2017. A novel approach to damage localisation based on bispectral analysis and neural network. Smart Struct. Syst. 20.
Coletta, G., Miraglia, G., Pecorelli, M., Ceravolo, R., Cross, E., Surace, C., Worden, K., 2019. Use of the cointegration strategies to remove environmental effects from data acquired on historical buildings. Eng. Struct. 183 https://doi.org/10.1016/j.engstruct.2018.12.044.
Cross, E.J., Worden, K., 2011. Approaches to nonlinear cointegration with a view towards applications in SHM. In: Journal of Physics: Conference Series. https://doi.org/10.1088/1742-6596/305/1/012069.
Dao, P.B., Staszewski, W.J., Barszcz, T., Uhl, T., 2018. Condition monitoring and fault detection in wind turbines based on cointegration analysis of SCADA data. Renew. Energy 116. https://doi.org/10.1016/j.renene.2017.06.089.
Davenport, A.G., 1961. The spectrum of horizontal gustiness near the ground in high winds. Q. J. R. Meteorol. Soc. 87 https://doi.org/10.1002/qj.49708737208.
DNV, G.L., 2017. DNVGL-RP-C205: Environmental Conditions and Environmental Loads. DNV GL Recommended Practice.
Drucker, H., Burges, C.J.C., Kaufman, L., Smola, A., Vapnik, V.N., 1996. Support Vector Regression Machines. NIPS.
Eidsvik, K.J., 1985. Large-sample estimates of wind fluctuations over the ocean. Boundary-Layer Meteorol. 32 https://doi.org/10.1007/BF00120931.
Engle, R.F., Granger, C.W.J, 1987. Co-integration and error correction: Representation, estimation, and testing. Econometrica 55, 251. https://doi.org/10.2307/1913236.
Ewins, D.J., 2000. Modal Testing: Theory, Practice and Application (Mechanical Engineering Research Studies: Engineering Dynamics Series). Research Studies Press Ltd.
Fathi, A., Esfandiari, A., Fadavie, M., Mojtahedi, A., 2020. Damage detection in an offshore platform using incomplete noisy FRF data by a novel Bayesian model updating method. Ocean Eng. 217 https://doi.org/10.1016/j.oceaneng.2020.108023.
Fuller, W.A., 2008. Introduction to statistical time series. In: Introduction to Statistical Time Series, second ed. https://doi.org/10.1002/9780470316917 Second Edition.
Gaudard, M., Ramsey, P.J., 1997. Introduction to statistical quality control. Technometrics 39, 331–332. https://doi.org/10.1080/00401706.1997.10485124.
Hasselmann, K., Barnett, T.P., Bouws, E., Carlson, H., Cartwright, D.E., Eake, K., Euring, J.A., Gicnapp, A., Hasselmann, D.E., Kruseman, P., Meerburg, A., Mullen, P., Olbers, D.J., Richren, K., Sell, W., Walden, H., 1973. Measurements of Wind-Wave Growth and Swell Decay during the Joint North Sea Wave Project (JONSWAP).
Heidrun - oil and gas field in the Norwegian Sea - Equinor [WWW Document], n.d. URL https://www.equinor.com/energy/heidrun (accessed 4.18.23).
Hillis, A.J., Courtney, C.R.P., 2011. Structural health monitoring of fixed offshore structures using the bicoherence function of ambient vibration measurements. J. Sound Vib. 330 https://doi.org/10.1016/j.jsv.2010.09.019.
Ibrahim, S.R., Brincker, R., Asmussen, J.C., 1996. Modal parameter identification from responses of general unknown random inputs. In: Proceedings of the 14th International Modal Analysis Conference (IMAC XIV).
Khosravan, A., Asgarian, B., Shokrgozar, H.R., 2021. Improved Modal Strain Energy Decomposition Method for damage detection of offshore platforms using data of sensors above the water level. Ocean Eng. 219 https://doi.org/10.1016/j.oceaneng.2020.108337.
Liang, Y., Li, D., Song, G., Feng, Q., 2018. Frequency Co-integration-based damage detection for bridges under the influence of environmental temperature variation. Measurement 125. https://doi.org/10.1016/j.measurement.2018.04.034.
Liu, G., Zhai, Y., Leng, D., Tian, X., Mu, W., 2017. Research on structural damage detection of offshore platforms based on grouping modal strain energy. Ocean Eng. 140 https://doi.org/10.1016/j.oceaneng.2017.05.021.
Liu, K., Yan, R.J., Guedes Soares, C., 2018. Damage identification in offshore jacket structures based on modal flexibility. Ocean Eng. 170 https://doi.org/10.1016/j.oceaneng.2018.10.014.
Mojtahedi, A., Hokmabady, H., Yaghubzadeh, A., Mohammadyzadeh, S., 2020. An improved model reduction-modal based method for model updating and health monitoring of an offshore jacket-type platform. Ocean Eng. 209 https://doi.org/10.1016/j.oceaneng.2020.107495.
Morison, J.R., Johnson, J.W., Schaaf, S.A., 1950. The force exerted by surface waves on piles. J. Petrol. Technol. 2 https://doi.org/10.2118/950149-g.
Naderpour, H., Fakharian, P., 2016. A synthesis of peak picking method and wavelet packet transform for structural modal identification. KSCE J. Civ. Eng. 20 https://doi.org/10.1007/s12205-016-0523-4.
Nichol, S., Carriveau, R., Miller, L., Ting, D.S.K., Romanic, D., Costache, A., Hangan, H., 2021. Experimental investigation of the movement of an offshore floating platform in straight wind, tornadic wind, and downburst conditions. Energies 14. https://doi.org/10.3390/en14072020.
Norwegian Oil and Gas Association, 2015. 40-Norwegian Oil and Gas Recommended Guidelines for Offshore Loading Shuttle Tankers.
Peeters, B., Roeck, G. De, 2001. Stochastic system identification for operational modal analysis: a Review. J. Dyn. Syst., Measurement and Control, Transac. ASME 123. https://doi.org/10.1115/1.1410370.
Perman, R., 1991. Cointegration: an introduction to the literature. J. Econ. Stud. 18 https://doi.org/10.1108/EUM0000000000151.
Pezeshki, H., Adeli, H., Pavlou, D., Siriwardane, S.C., 2023. State of the art in structural health monitoring of offshore and marine structures. In: Proceedings of the Institution of Civil Engineers: Maritime Engineering 176. https://doi.org/10.1680/jmaen.2022.027.
Ruotolo, R., Surace, C., Worden, K., 2000. Application of two damage detection techniques to an offshore platform. Shock Vib. Digest 32.
Rytter, A., 1993. Vibrational based inspection of civil engineering structures. Fracture and Dynamics. https://doi.org/10.1016/j.jsv.2016.06.047.
Shen, C., Liu, Z., Li, Y., 2013. Nonlinear cointegration analysis based on support vector machines and its application to the connection between financial markets. https://doi.org/10.2991/cse.2013.28.
Shen, J., Liu, F., Li, H., Xu, L., Liang, B., 2015. Assessment of the damages occurring between two adjacent measurements for an aging offshore platform. Ocean Eng. 109 https://doi.org/10.1016/j.oceaneng.2015.09.024.
Shi, H., Worden, K., Cross, E.J., 2016. A nonlinear cointegration approach with applications to structural health monitoring. In: Journal of Physics: Conference Series. https://doi.org/10.1088/1742-6596/744/1/012025.
Sohn, H., 2007. Effects of environmental and operational variability on structural health monitoring. Phil. Trans. Math. Phys. Eng. Sci. 365 https://doi.org/10.1098/rsta.2006.1935.
Sohn, H., Farrar, C.R., Hunter, N.F., Worden, K., 2001. Structural health monitoring using statistical pattern recognition techniques. J. Dyn. Syst., Measurement and Control, Transac. ASME 123. https://doi.org/10.1115/1.1410933.
Sousa Tomé, E., Pimentel, M., Figueiras, J., 2020. Damage detection under environmental and operational effects using cointegration analysis – application to experimental data from a cable-stayed bridge. Mech. Syst. Signal Process. 135 https://doi.org/10.1016/j.ymssp.2019.106386.
Statfjord Field, North Sea [WWW Document], n.d.. NS ENERGY. URL https://www.nsenergybusiness.com/projects/statfjord-field-north-sea/(accessed 5.6.23)..
Surace, C., Worden, K., 1998. Using novelty detection to diagnose damage in structures with time-varying parameters. In: Proceedings of the International Conference on Damage and Fracture Mechanics.
Surace, C., Worden, K., 2010. Novelty detection in a changing environment: A negative selection approach. Mech. Syst. Signal Process 24. https://doi.org/10.1016/j.ymssp.2009.09.009.
Tipping, M.E., 2001. Sparse bayesian learning and the relevance vector machine. J. Mach. Learn. Res. 1.
Varahram, S., Jalali, P., Sadeghi, M.H., Lotfan, S., 2019. Experimental study on the effect of excitation type on the output-only modal analysis results. Trans. FAMENA 43. https://doi.org/10.21278/TOF.43303.